

DESIGN OF A WIDEBAND VIVALDI ANTENNA ARRAY FOR THE SNOW RADAR

by

Raviprakash Rajaraman

B.E. (Electronics & Communications Engg.), Coimbatore Inst. of Tech, India, 2001

Submitted to the Department of Electrical Engineering and Computer Science and the Faculty of the Graduate School of the University of Kansas in partial fulfillment of the requirements for the degree of Master of Science.

Dr. Prasad Gogineni

Dr. Glenn Prescott

Dr. Pannir Kanagaratnam

2nd February, 2004

Date project defended

To my parents and sisters

ACKNOWLEDGEMENTS

I wish to express sincere thanks to my advisor, Dr. Prasad Gogineni, for giving me this opportunity to work on this project. I would like to thank Dr. Glenn Prescott for agreeing to serve on my defense committee.

I would also like to extend my gratitude to Dr. Pannir Kanagaratnam for not only serving on my committee, but also for the invaluable time and effort that he has put into this project. I would like to acknowledge that without his advice this project would not have been completed in time. I also take this opportunity to thank Dennis Sundermeyer for always being ready to help me out with the antenna assembly and also doing an exceptional job at it.

It is also my pleasure to thank Sudarsan for being such a great help in making measurements with the antenna both inside and outside the building. I would like to extend my thanks Timothy Rink and Bharath for helping me with the pattern measurements on the roof in not so friendly weather. I also thank Harish and Abhinay for helping me with the measurements.

I am grateful to John Paden and Dr. Dawood for being ready to answer my numerous questions anytime. Thanks are also due to all the people at Ansoft technical support for assisting me with the simulations.

I would like to extend a word of thanks to all my friends who have made my stay in Lawrence a pleasant and memorable one. I like to thank my parents and sisters, whose unlimited love and support has made this effort possible. Finally, I thank Almighty God for always being there to guide me through thick and thin.

ABSTRACT

A 2-8 GHz FM-CW based radar was built at the University of Kansas to measure the thickness of snow cover over sea ice. Two double-ridged waveguide TEM horn antennas were used to transmit and receive the radar signals. Although these antennas performed well for ground-based radar measurements it would be prudent to seek an antenna with a narrower beamwidth for airborne experiments. A narrow beamwidth antenna would be required for airborne applications to reduce the effects of off-angle clutter from the snow surface. However, an array of horn antennas would be bulky due to its relatively large size. It was then decided to design an array of Vivaldi antennas to obtain a narrower beamwidth. The Vivaldi is extremely light weight and could be easily developed as an array with relatively lower cost than the horn antennas.

The characteristics of the Vivaldi antenna were understood through extensive simulations performed in Ansoft HFSS after which the Vivaldi antenna was built and tested at the RSL. The gain and the S11 of the single element were found to be quite poor. Subsequently, a 12-element array was built. A metal plate was fixed to the back of the antenna to reflect any signals going in the backward direction. The S11 of the array was found to be better than -7 dB almost throughout the desired bandwidth, except at about 3 GHz. The pattern measurements were also done on this array using the antenna range (KUAR) on the roof of the building. These revealed a fairly narrow beamwidth on the E-plane and a wide one on the H-plane throughout the bandwidth. The average half-power beamwidth in the E-plane for the Vivaldi was 15° while it was about 50° for the TEM horn. The realized gain was found to vary between 8.5 dB at the lower end to about 16 dB at the higher end of the bandwidth. However, since the measurements were done in

less than ideal conditions, they were prone to errors, both human and otherwise. Most of the design requirements for this antenna were met. A few changes to the design with regards to impedance matching would make it ready for installation and integration with the rest of the radar equipment.

Table of Contents

Chapter 1 Introduction	1
1.1 Significance of snow thickness measurements over sea ice	1
1.2 Objective	2
1.3 Organization.....	3
Chapter 2 Vivaldi antenna	5
2.1 Characteristics.....	5
2.1.1 Construction.....	5
2.1.2 Principle of operation.....	6
2.1.3 Radiation	7
2.1.4 Bandwidth	7
2.2 Taper profiles	9
2.2.1 Types.....	9
2.2.2 Effect of curvature on the TSA.....	10
2.3 Feeding techniques.....	10
2.3.1 Coaxial-slotline transition.....	11
2.3.2 Microstrip-slotline transition	13
2.4 Summary	16
Chapter 3 Antenna design.....	17
3.1 Parameter study: An overview.....	17
3.2 Introduction.....	18
3.3 Substrate material.....	20
3.4 Feed mechanism.....	21

3.4.1 Background	21
3.4.2 Stripline-slotline transition.....	22
3.5 Taper design.....	29
3.6 Array design.....	30
3.6.1 Introduction.....	30
3.6.2 Array factor.....	31
3.6.3 Mutual Coupling	32
3.6.4 Linear Vivaldi array.....	33
3.7 Fabrication	35
3.8 Summary	36
Chapter 4 Simulation	38
4.1 Introduction.....	38
4.2 Description.....	39
4.2.1 Single element Vivaldi antenna	40
4.2.2 Infinite Vivaldi array with backplane	46
Chapter 5 Test & Measurement	53
5.1 Background.....	53
5.2 Power divider	54
5.3 Reflection measurements.....	56
5.3.1 Test setup	56
5.3.1 Single element Vivaldi antenna	57
5.3.2 Twelve-element Vivaldi array	60
5.4 Pattern measurements	67

5.4.1 Introduction.....	67
5.4.2 Setup	69
5.4.3 Polarization	72
5.4.4 Gain measurement	73
5.4.5 Radiation pattern measurements	75
5.5 Summary.....	83
Chapter 6 Summary and recommendations	85
6.1 Summary.....	85
6.2 Recommendations.....	88
Chapter 7 References	90
Chapter 8 Appendix	93
8.1 Datasheets	93
8.2 Pictures.....	93

List of Figures

Figure 2-1: Vivaldi antenna	5
Figure 2-2: Typical radiation pattern of TSAs[10]	7
Figure 2-3: Different taper-styles of the TSA: (a) Exponential (Vivaldi); (b) Linear-constant; (c) Tangential; (d) Exponential-constant; (e) Parabolic; (f) Step-constant; (g) Linear; (h) Broken-linear [12]	9
Figure 2-4: Different feed techniques: (a) Coaxial line;(b) Microstrip; (c) CPW; (d) air-bridge/GCPW, (e) FCPW/centre-strip, (f) FCPW/notch [12]	11
Figure 2-5: Coax-slotline feed	12
Figure 2-6: Coax-fed Vivaldi antenna [17]	12
Figure 2-7: Microstrip-slotline transition	13
Figure 2-8: Microstrip-slotline transition using radial stubs [20]	14
Figure 2-9: Antipodal Vivaldi antenna [22]	15
Figure 2-10: Balanced antipodal Vivaldi antenna [24]	16
Figure 3-1: Vivaldi notch element	19
Figure 3-2: Microstrip-slotline transition	22
Figure 3-3: Stripline Triplate Structure	24
Figure 3-4: Slotline structure – end and top views	25
Figure 3-5: Double transition in HFSS ^[R]	27
Figure 3-6: (a) S11; (b) S21 - Simulation results of the transition	28
Figure 3-7: Vivaldi antenna parameters	29
Figure 3-8: AF of 2 isotropic sources with identical amplitude and phase currents spaced one-half wavelength apart	32

Figure 3-9: AF of an endfire 12-element linear array at 8 and 2 GHz.....	34
Figure 3-10: (a) Single element Vivaldi antenna; (b) 12-element Vivaldi array	36
Figure 4-1: Single element Vivaldi model.....	40
Figure 4-2: S11 of single element Vivaldi antenna	41
Figure 4-3: E-field plot of structure	41
Figure 4-4: E & H field intensity vectors.....	42
Figure 4-5: E & H plane cuts of Vivaldi antenna	44
Figure 4-6: E & H plane rectangular plots.....	45
Figure 4-7: Infinite array Vivaldi model.....	48
Figure 4-8: E and H plane cuts	51
Figure 4-9: HPBW of 12 element linear array.....	51
Figure 5-1: Characteristics of 12-way power divider	55
Figure 5-2: S11 measurement setup.....	56
Figure 5-3: S11 comparison.....	58
Figure 5-4: Reflection from target at 7ft from antenna.....	58
Figure 5-5: Test setup for array antenna	61
Figure 5-6: Array reflection measurements	62
Figure 5-7: Vivaldi array setup	63
Figure 5-8: Time-gating of reflected signal	65
Figure 5-9: Radiation pattern measurement setup	68
Figure 5-10: Antenna Range setup	71
Figure 5-11: Azimuth & Elevation cuts at 2.5 GHz	79
Figure 5-12: Azimuth & Elevation cuts at 5 GHz	81

Figure 5-13: Azimuth and elevation cuts at 7.5 GHz	82
Figure 8-1: Vivaldi antenna array in (a) Horizontal, and (b) Vertical polarization.....	94
Figure 8-2: Double-ridged waveguide horn - Vertically polarized	94

List of Tables

Table 3-1: Dielectric characteristics	21
Table 3-2: Stripline parameters.....	23
Table 3-3: Transition parameters	27
Table 3-4: Antenna features.....	37
Table 4-1: General simulation settings in HFSS.....	40
Table 4-2: Antenna parameters at 6 GHz	46
Table 5-1: Network Analyzer settings	59
Table 5-2: Single element antenna - reflection measurement.....	60
Table 5-3: Power ratio comparison.....	67
Table 5-4: Antenna range setup features	72
Table 5-5: Horn gain measurements	75
Table 5-6: Vivaldi gain measurements	75
Table 5-7: Measurement results.....	84

Chapter 1 Introduction

1.1 Significance of snow thickness measurements over sea ice

Sea ice plays a crucial role in the global climate system. As such, changes in sea ice extent can foretell changes in the global climate system [1]. In addition, sea ice also has an important role in the polar ecosystem. It is home to various algae and protozoa and serves as a platform for seals, penguins and polar bears [2].

Due to its low thermal conductance, sea ice limits the amount of heat that is exchanged between the ocean and the atmosphere. This is especially important in winter as it helps the ocean to preserve its thermal energy. The presence of snow cover further reduces the thermal loss from the ocean as it acts as a blanket to retain the heat. The snow cover also regulates the amount of solar radiation that is absorbed by the underlying media. Like any white surface, snow also reflects most of the solar radiation due its high reflectivity. The degree of reflectivity is a measure of its albedo. A high albedo indicates a highly reflective medium. Due to its high albedo, snow cover reflects about 80% of the solar radiation back to space. This helps to keep the polar region colder than what it would be if there was no snow or ice cover.

By continuously monitoring the sea ice extent and snow cover over the polar region scientists will be able to understand the dynamics of snow, ice and ocean interaction. This will also help scientists develop models to predict the changes that may occur in the global climate. Due to these factors it is important for us to be able to observe the sea ice extent and snow cover over the polar regions. The only effective means of doing this on a global scale is via remote sensing techniques.

1.2 Objective

Markus et al. [3] have developed an algorithm to estimate the thickness of snow cover from passive microwave data. However there are currently no effective means to test and validate the algorithm over the footprint of a space-borne radiometer. A prototype ultra wideband Frequency Modulated Continuous Wave (FMCW) radar has been developed at the University of Kansas by Wong [4] to measure the thickness of snow over sea ice. This radar operates from 2 to 8 GHz and has a vertical resolution of about 4 cm in snow. The prototype was designed to operate on a sled to collect data over snow-covered sea ice. TEM horn antennas were employed for transmitting and receiving the signals. The transmitter and receiver, along with the antennas, were mounted approximately 1 m above the top snow level. This radar was successfully tested in a ground-based experiment during the fall of 2003 in Antarctica. While the TEM horn antennas were adequate for a ground-based experiment it would be prudent to seek an antenna configuration with a narrower beamwidth for airborne application. A narrow beamwidth antenna would be required for airborne applications to reduce the effects of off-angle clutter from the snow surface.

A narrow beamwidth can be obtained by arranging the antenna in an array configuration. The TEM horn is too bulky and would have been difficult to use in an array configuration owing to its relatively large size. The objective of this project is to design an array antenna that would operate in the 2 to 8 GHz frequency range and that is not as bulky as the horn. The Vivaldi antenna has a number of characteristics favorable for this application. The Vivaldi antenna belongs to the class of tapered slot antennas with an exponential taper profile and are aperiodic continuously scaled traveling-wave antenna

structures^[5]. Exceedingly high bandwidths, of the order of more than two octaves could be reached. The antenna could be designed in such a way that very low beamwidths could be attained. When designed as an array, the beam switching and shaping could also be done based on the requirements. Moreover, the cost of buying a horn antenna off the shelf was very high and this was taken care of by the Vivaldi design which was completely fabricated in the lab.

1.3 Organization

The report has been divided into a total of six chapters.

Chapter 2 begins with an introduction of the basic Vivaldi antenna. The characteristics and design considerations will give an insight into the operations of the antenna. The different types of tapers and their effects on the antenna performance have been discussed. A literature study was also done on the two major feeding techniques at the end of the chapter.

Chapter 3 provides an in depth look into the principles of design of the Vivaldi antenna. The choice of the substrate, the type of feed mechanism and other design issues are discussed here. The stripline and the slotline designs are discussed separately with appropriate equations. The design procedure for the linear Vivaldi array is also given. Finally, the procedure for fabricating the antenna has been described.

Chapter 4 discusses in detail the various simulations that were done in Ansoft HFSS^[R] [6] to understand the performance of the antenna and how the different design parameters affect it. The S-parameter and the field pattern plots have been generated from the simulation and have been displayed in this chapter.

Chapter 5 talks about the various measurements and calculations that were made with both the single element as well as with the linear array antenna. Measurements were made both inside the lab as well as on the roof.

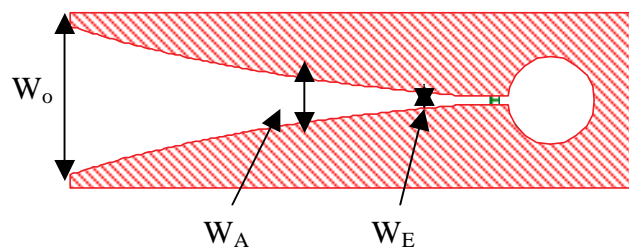
Chapter 6 summarizes the whole project and provides a few areas to improve for the future.

Chapter 2 Vivaldi antenna

This chapter begins with a discussion of the typical characteristics of the Tapered-Slot Antenna (TSA). The Vivaldi antenna is a special type of TSA with an exponential flare profile. It is then followed by a review of the various design principles to be taken into consideration in the process of constructing this antenna. Finally, there is a brief discussion on the different design methodologies that were proposed in the literature.

2.1 Characteristics

2.1.1 Construction



W_E - Input slot width

W_A - Slot width at radiating area

W_O - Output slot width

Figure 2-1: Vivaldi antenna

The Vivaldi (Figure 2.1) is a member of a class of aperiodic continuously scaled traveling-wave antenna structures^[5]. The terms “tapered-notch”, “flared-slot”, “tapered-slot” antennas have been used interchangeably in the literature. These antennas consist of a tapered slot etched onto a thin film of metal. This is done either with or without a dielectric substrate on one side of the film. Besides being efficient and lightweight, the

more attractive features of TSAs are that they can work over a large frequency bandwidth and produce a symmetrical end-fire beam with appreciable gain and low side lobes^[7]. An important step in the design of the antenna is to find suitable feeding techniques for the Vivaldi.

Understanding the characteristics of the Vivaldi is fundamental and would help a great deal in designing the antenna. From research journals on the TSA, we can confirm that TSAs generally have wide bandwidth, high directivity and are able to produce symmetrical radiation patterns^[8].

The feature that is common to all the different designs of this antenna is the exponentially flared slot. This aspect is particularly analogous to the standard TEM horn antenna^[9] – the width of the flare increases with distance from the antenna feed. In fact, we could say that the Vivaldi is the printed-circuit equivalent of the horn. The wave-guiding structure here is the printed slotline that is tapered exponentially outwards. A more detailed procedure of construction is explained in a later section.

2.1.2 Principle of operation

As stated earlier, the Vivaldi antenna is a type of a traveling-wave antenna of the “surface-type”. The waves travel down the curved path of the flare along the antenna. In the region where the separation between the conductors is small when compared to the free-space wavelength, the waves are tightly bound and as the separation increases, the bond becomes progressively weaker and the waves get radiated away from the antenna^[5].

This happens when the edge separation becomes greater than half-

Radiation from high-dielectric substrates is very low and hence for antenna applications significantly low dielectric constant materials are chosen.

2.1.3 Radiation

The tapered-slot antennas utilize a traveling wave propagating along the antenna structure

well as $v_{ph} = c$ [5]. Therefore, the Vivaldi is characterized by

radiation in the endfire direction (Figure 2.2) at the wider end of the slot in preference to

$v_{ph} = c$ relates to the case of the antenna with air as the dielectric and consequently the beamwidth and the sidelobe level are considerably

greater than with a dielectric present. Also, the phase velocity and the guide wavelength

λ_g vary with the change in the thickness, dielectric constant and taper design. Typically,

the beamwidth in the E-plane and the H-plane patterns are almost the same.

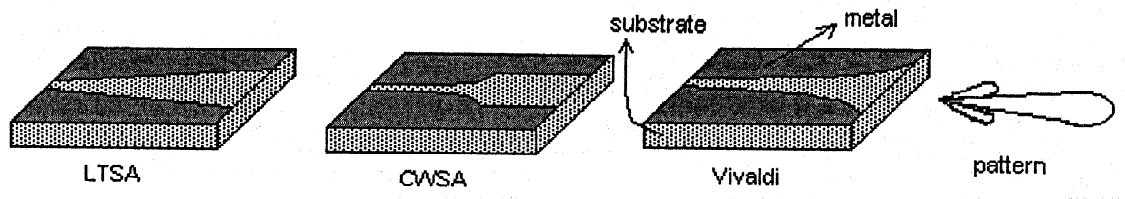


Figure 2-2: Typical radiation pattern of TSAs[10]

2.1.4 Bandwidth

At different frequencies, different parts of the antenna radiate, while the radiating part is constant in wavelength [5]. Thus the antenna theoretically has an infinite bandwidth of

operation and can thus be termed frequency independent. As the wavelength varies,

radiation occurs from a different section which is scaled in size in proportion to the

wavelength and has the same relative shape. This translates into an antenna with very

large bandwidth. Again referring to Figure 2.1 it can be seen that the Vivaldi antenna is

divided into two areas:

- a propagating area defined by $W_E < W < W_A$
- a radiating region defined by $W_A < W < W_O$

Where,

W - Slot width

W_E - Input width

W_A - Slot width at radiating area

W_O - Output width

The original Vivaldi antenna proposed by Gibson ^[5] employed a taper that opened up real fast thus providing an almost constant beamwidth over the entire frequency range of about two octaves when plotted with frequency or normalized length. For antennas with smaller opening angles, the beam width becomes dependent upon the frequency, as predicted by Zucker^[11].

Theoretically, the TSA is capable of having an operating bandwidth within a frequency range of 2 GHz to 90 GHz while practically the operating bandwidth is limited by the transition from the feeding transmission line to the slot line of the antenna and by the finite dimensions of the antenna. Thus to achieve a wider bandwidth, it is imperative for the designer to have in mind the following two aspects:

- The transition from the main input transmission line to the slot line for feeding the antenna. This is designed for a low reflection coefficient to match the potential of the antenna.
- The dimensions and shape of the antenna, to obtain the required beam width, side lobes and back lobes, over the operating range of frequencies.

2.2 Taper profiles

2.2.1 Types

Many taper profiles exist for a normal TSA. Figure 2.3 shows different planar designs and we can observe that each antenna differs from the other only in the taper profile of the slot^[12]. Planar tapered slot antennas have two common features. The radiating slot acts as the ground plane for the antenna and the antenna is fed by a balanced slotline. However, drawbacks for a planar TSA come in the form of using a low dielectric constant substrate and obtaining an impedance match for the slotline. By fabricating on a low dielectric constant substrate, relatively high impedance is obtained for the slotline. If a microstrip feed is chosen, it makes matching very difficult. Thus, the microstrip to slot transition will limit the operating bandwidth of the TSA.

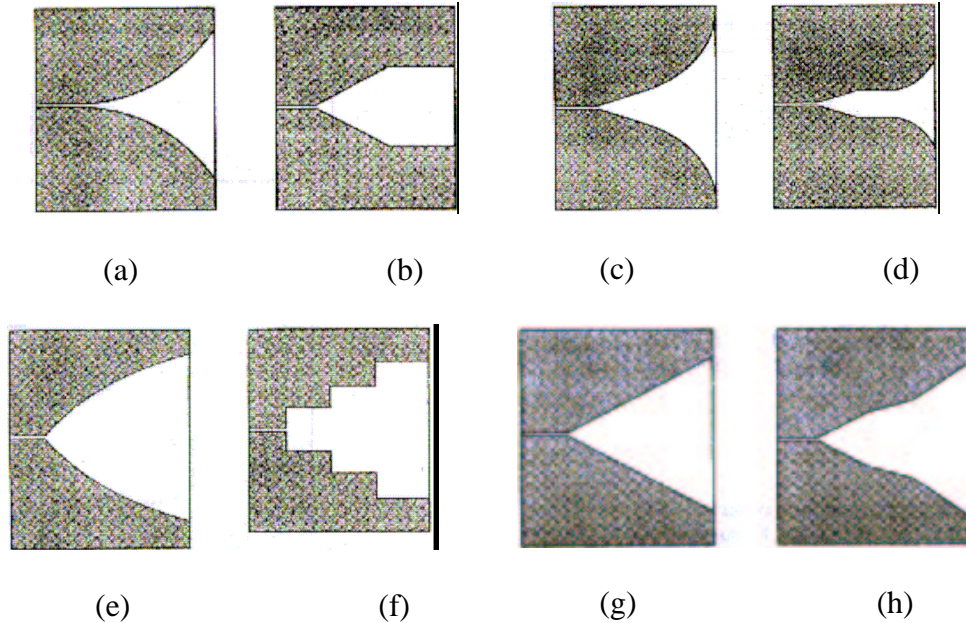


Figure 2-3: Different taper-styles of the TSA: (a) Exponential (Vivaldi); (b) Linear-constant; (c) Tangential; (d) Exponential-constant; (e) Parabolic; (f) Step-constant; (g) Linear; (h) Broken-linear [12]

2.2.2 Effect of curvature on the TSA

Experiments conducted by Lee and Simons^[13] have shown that the curvature of tapered profile has a significant impact on the gain, beamwidth and bandwidth of tapered slot antennas. In fact, it was shown that the half-power beamwidth (HPBW) on the E-plane increases with a decrease in the radius of curvature while the opposite is true on the H-plane. The cross polarization is generally improved with the decrease in the radius of the curvature except for the E-plane, which will not show any improvement. Also the authors have shown that the bandwidth of the antenna reduces with a decrease in the radius of curvature which is exactly the opposite of what we want to focus on.

2.3 Feeding techniques

In theory, the bandwidth of the Vivaldi antenna is infinite; the only limitation on the bandwidth is the physical size of the antenna and the fabrication capabilities. In fact, the feed determines the high frequency limit while the aperture size the low frequency limit^[14]. As discussed earlier, a proper feed structure design becomes essential to maximize the bandwidth.

Most microwave integrated circuits (MICs) are realized in microstrip transmission medium. However, the transmission medium best suited for feeding the TSA is a slotline. In order to couple microwave signals to the antenna from a planar microstrip circuit, a transition is needed. These transitions should be very compact and have low loss. Some feeding techniques and their transitions are shown in the Figure 2.5. The commonly used methods are the coaxial line feed and the microstrip line feed. These will be illustrated and discussed in the next two sub-sections.

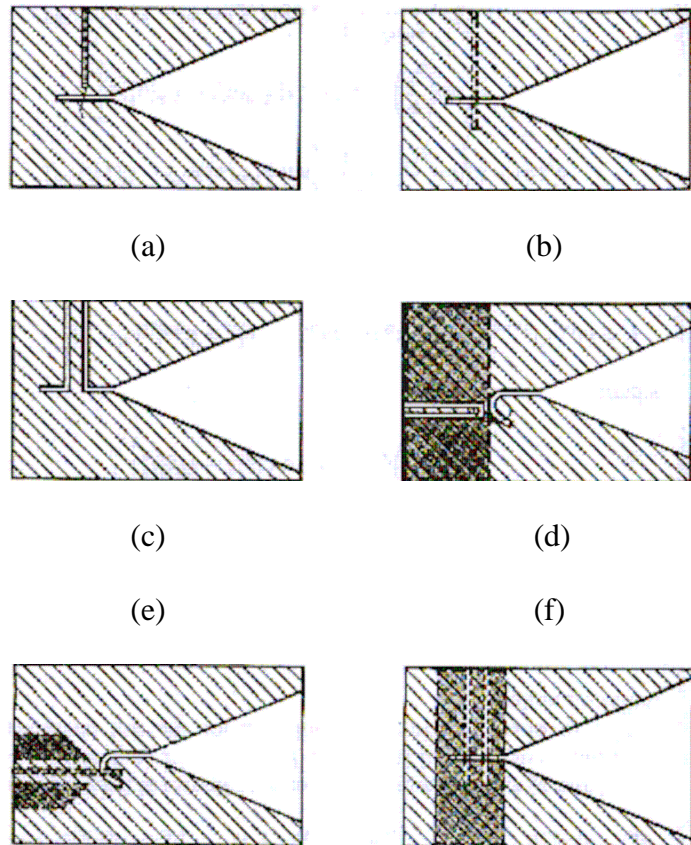


Figure 2-4: Different feed techniques: (a) Coaxial line;(b) Microstrip; (c) CPW; (d) air-bridge/GCPW, (e) FCPW/centre-strip, (f) FCPW/notch [12]

2.3.1 Coaxial-slotline transition

A coaxial line feed provides a direct path for coupling of fields across the slot^[14]. The transition consists of a coaxial line placed perpendicular at the end of an open circuited slot. The outer conductor of the cable is electrically connected to the ground plane on one side of the slot while the inner conductor of the coaxial line forms a semicircular shape over the slot^[16]. This is shown in Figure 2-5. However, designing slotlines with very low characteristic impedances is difficult as the width has to then be too narrow and hence etching becomes inaccurate.

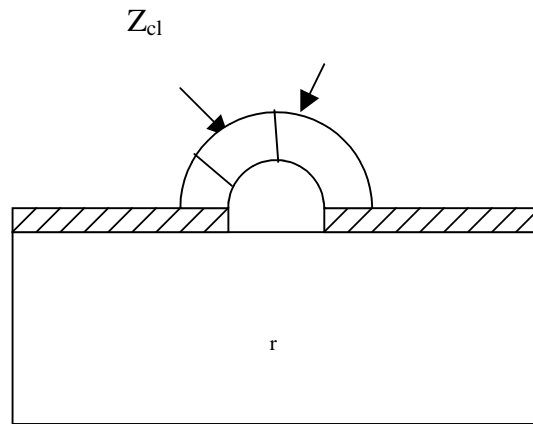


Figure 2-5: Coax-slotline feed

Using double-clad, i.e., etching the slotline on both sides of the substrate, rather than single-clad, reduces the characteristic impedance of the slotline so that better matching with the coaxial line becomes possible. Weedon et al^[17] have used this idea to design a Vivaldi antenna (Figure 2.6) and has shown a pattern bandwidth of at least 9:1.

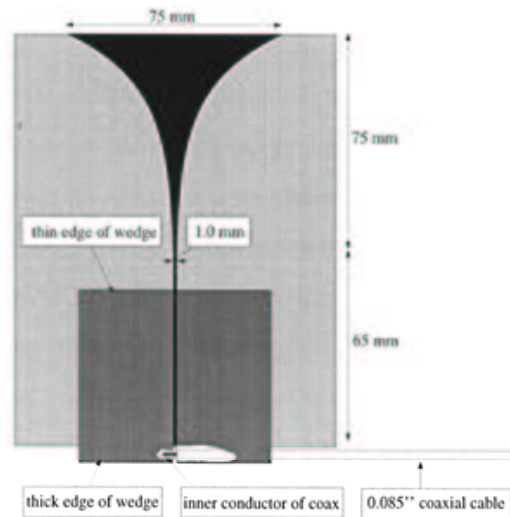


Figure 2-6: Coax-fed Vivaldi antenna [17]

2.3.2 Microstrip-slotline transition

As stated earlier, the microstrip transmission medium is used extensively in MICs. However, research shows that the slotline would be the medium best suited for feeding the TSA. The microstrip is an unbalanced transmission line while the medium used for feeding the Vivaldi is a slotline which is a balanced medium. The success of the whole design is thus hinged on the design of a proper balun for this transition. The objective is thus to design a balun that would work over a wide frequency range or ideally be frequency independent.

A microstrip to slot transition consists of a slot, etched on one side of the substrate, crossing an open circuited microstrip line, located on the opposite side, at a right angle^[16]. The slot extends to one quarter of a wavelength ($s/4$) beyond the microstrip and $m/4$ beyond the slot^[18] as shown in Figure 2.7. A more detailed description of the transition and the design procedure is given in the next chapter.

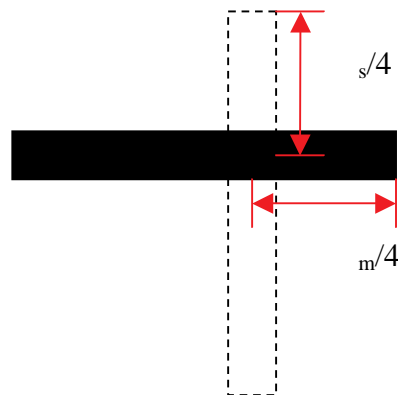


Figure 2-7: Microstrip-slotline transition

A major drawback for this kind of a transition is its reduced operating bandwidth. A number of ways have been suggested in the literature that improves this microstrip-slotline transition [18], [19], [20]. These methods have not only shown a marked improvement in the bandwidth but sometimes have shown better radiation characteristics. These variations have been discussed below in brief. A more detailed description is available with the stated references and would serve to complete the understanding of the concepts involved.

2.3.2.1 Non-uniform stubs

Schuppert^[18] proposed the use of circular quarter-wave stubs in the design of microstrip-slotline transitions. This enabled him to obtain a more wideband transition than from the transitions with straight stubs. Subsequently, with the help of equations provided in [15], [18] and [19], Sloan et al^[20] came up with the idea of using radial stubs instead of the circular ones as shown in Figure 2.8. A detailed design procedure is given in the next chapter.

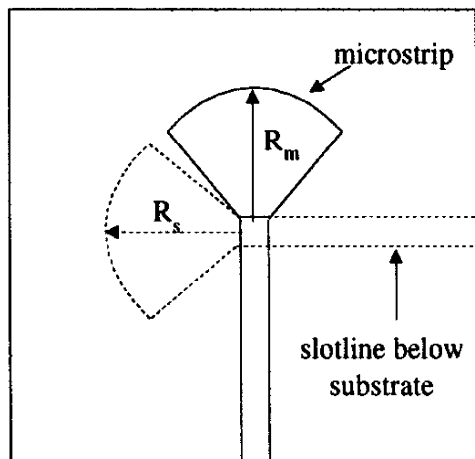


Figure 2-8: Microstrip-slotline transition using radial stubs [20]

2.3.2.2 Antipodal slotline

The symmetric double-sided slotline, also referred to as the antipodal slotline was first suggested by Gazit^[21]. In this case, the transition from the microstrip to the slotline was realized through a parallel stripline as shown in Figure 2.9. The microstrip was used as the input feed, the slotline for radiating purposes while the paired-strip served primarily as the transition region thus critically affecting the antenna performance. This design also helped avoid the slot hole that was necessary in the earlier designs. Noronha et al^[22] have used this idea to construct a Vivaldi antenna and have shown good results over a wide frequency range. They have also empirically discovered that the transition region should be three to five wavelengths long to prevent a sharp discontinuity between the feed and the radiating regions.

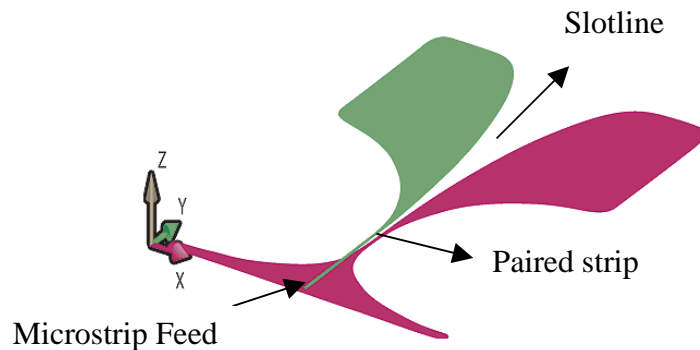


Figure 2-9: Antipodal Vivaldi antenna [22]

2.3.2.3 Balanced antipodal slotline

It was found that the previous design did not have a really good cross-polarization characteristic. This was even more pronounced at high frequencies, when the angle of the E-field skew with respect to the physical axis of the antenna increased considerably. Hence, there was a severe polarization tilt as the frequency of operation was increased.

Langley et al^[23] came up with a solution – the balanced antipodal Vivaldi antenna as shown in Figure 2.10.

The improvement in the cross-polarization performance was brought about by converting the usual antipodal Vivaldi into a triplate-based structure, by adding an additional dielectric and metallization layer that balances the E-field distribution in the flared-slot. The antenna starts in a stripline. One side of the board has the input track that is then flared to produce one half of a conventional Vivaldi. On the other side, the ground planes are reduced to a balanced set of lines that are flared-out in the opposite direction to form the overall balanced structure.

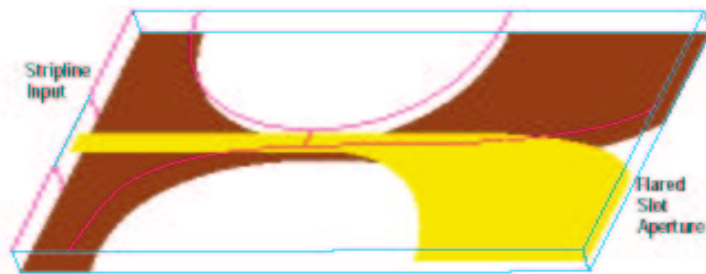


Figure 2-10: Balanced antipodal Vivaldi antenna [24]

2.4 Summary

This chapter has presented the characteristics and design considerations of a tapered slot antenna. Various taper profiles and feeding techniques were described and illustrated to give the antenna designer different options while designing a TSA. The effects of the various taper profiles on the bandwidth of the antenna were also highlighted. Finally, the transition design for the two common feeding techniques, coaxial line and microstrip line, were explored. With the knowledge of the facts presented in this chapter, the Vivaldi antenna could be designed and the design procedure is explained in the next chapter.

Chapter 3 Antenna design

This chapter describes the step-by-step procedure to design a Vivaldi antenna based on the specifications for the antenna. The stripline-fed Vivaldi antenna was chosen from all the other possible designs mainly because of the varied research accomplished on it. Also, not much work has been done on antenna arrays with feed mechanisms other than the stripline feed. A single-element antenna was first designed, fabricated and tested before developing a twelve-element linear array. This design has been based on the parameter study of the stripline-fed Vivaldi antenna arrays performed by Schaubert^[25].

3.1 Parameter study: An overview

As will be stated frequently in this document, the parameter study performed by Schaubert and Shin has been followed extensively in this design. The objective of the study was to analyze the various design parameters of the stripline-fed Vivaldi array antennas so that the wideband performance could be improved in a systematic procedure. The following were some of the parameters taken into consideration in the parameter study:

- Diameter of the slotline cavity and the stripline stub
- Input stripline and slotline width
- Taper profile
- Aperture height

The effect of varying these parameter values on the antenna performance (S11 and pattern) was discussed. Particularly, it was found out that through proper change in the design parameters, the antenna resistance could be increased and subsequently resulting

in a decrease in the minimum operating frequency of the antenna. The higher end of the bandwidth was set by the onset of grating lobes and hence only way to improve the bandwidth was by decreasing the lower cutoff. Thus the parameters were varied one at a time, with all others being constant, and the subsequent effect on the antenna impedance in a large array was predicted. Hence, this study helps the antenna designer by identifying some of the most important relationships between the design of the antenna and the performance of each of the elements in an array.

The above parameters were studied for different combinations of substrate thickness and stripline & slotline characteristic impedances. Of all the different design possibilities that were tested in the study, the one that was claimed to have the largest bandwidth and at the same time, displayed a better performance (S_{11} / antenna resistance) was chosen for the actual design. The reader is referred to the stated publication [25] for greater detail.

3.2 Introduction

The stripline-fed Vivaldi notch antenna comprises:

- The stripline-to-slotline transition.
- The stripline open circuit stub and slotline short circuit cavity.
- The radiating tapered slot.

Figure 3.1 is a snapshot of the triplate-structured Vivaldi notch element as modeled in HFSS. The outside layers, viz., the top and the bottom layers (in red) are identical tapered slotlines which also act as ground planes for this antenna. The middle layer is the stripline plane (in green) that is used as the connection to the signal input or any test equipment. These three layers together form the Vivaldi-notch antenna. The input signal is fed to the stripline input and is then magnetically coupled to the slotline on either sides of the

board. The input impedance of the antenna is dictated by the stripline while the operating bandwidth of the antenna is governed by the stripline-to-slotline transition.

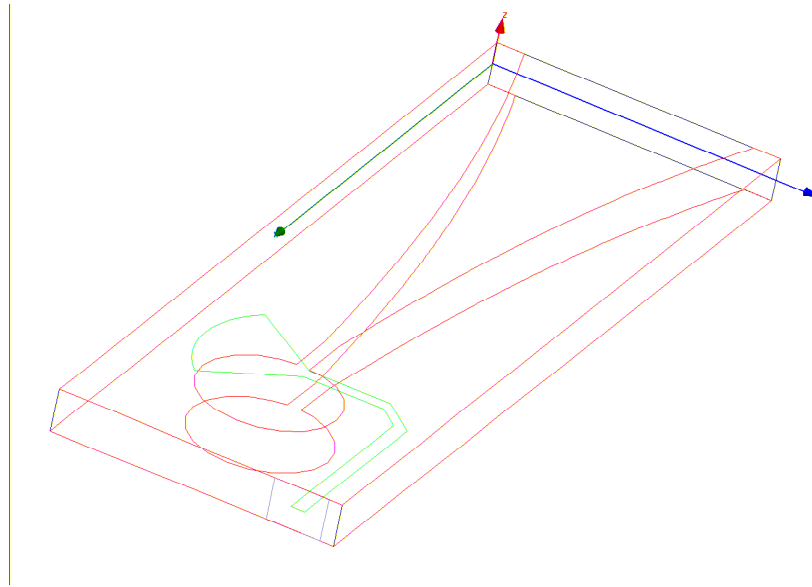


Figure 3-1: Vivaldi notch element

It was shown by Yngvesson^[9] and Gibson^[5] that single-element Vivaldi antennas work best when they are over a wavelength long and when the height of the antenna aperture is greater than one-half wavelength. In the case of arrays, on the other hand, good performance is obtained from antennas that are less than a wavelength long and when the element heights are much less than a wavelength. Typically, a single element in an array is unmatched almost throughout the bandwidth of interest. However, by proper array design, mutual coupling between the elements can be constructively used and very wideband behavior could be accomplished. The balanced-antipodal Vivaldi^[24] was also fabricated and tested, but its behavior in an array was not well documented. Hence this particular design was not considered.

The succeeding sections will discuss about the specifics of the design of the Vivaldi notch element. The design of a single-element is first considered after which the linear

array design is discussed. Antenna simulations done in Ansoft HFSS^[R] are discussed in the next chapter.

3.3 Substrate material

The choice of dielectric substrate plays an important role in the design and simulation of transmission lines as well as antennas. Some important dimensions of the dielectric substrate are, in no specific order:

- The dielectric constant.
- The dielectric loss tangent that sets the dielectric loss.
- The thickness of the copper surface.
- The thermal expansion and conductivity.
- Cost and manufacturability.

There are numerous types of substrates that can be used for the design of antennas. They often have different characteristics and their dielectric constants normally range from 2.2

ϵ_r provide better efficiency and a wider bandwidth. However, using thin substrates with high dielectric constant would result in smaller antenna size. But this also results negatively on the efficiency and bandwidth. Therefore, there must be a design trade-off between antenna size and good antenna performance^[26].

There are basically two types of losses that occur in any microstrip transmission line – the conductor and the dielectric losses, both of which increase with frequency. At low frequencies, the conductor losses dominate while at higher frequencies the loss due to the dielectric starts to become predominant. Dielectric loss is related to the fact that all dielectrics contain polarized molecules that move in the presence of EM fields. High-

frequency fields oscillate very quickly and as the polar molecules move in sync with the field, they begin to heat the dielectric material. There's only one possible source for the heat — the energy of the signal itself. It turns out that dielectric loss increases relentlessly with higher frequencies and in direct proportion to signal frequency.

Hence, to keep the dielectric losses low at the frequency of operation, the low-dielectric

$\epsilon_r = 2.22$) Rogers Duroid^[R] 5880 PTFE material with a low loss-tangent (0.0009) was chosen for this design. Table 3.1 gives a gist of the major properties of the material. A datasheet with more details on the different electrical and mechanical characteristics is provided in the Appendix of this report.

Characteristic	Value
Dielectric thickness	2*0.062"
ϵ_r	2.22
	0.0009
Thermal coefficient	-125 ppm/°C
Thermal conductivity	0.20 W/m/K
Conductor thickness	1 oz. (1.4 mil)

Table 3-1: Dielectric characteristics

3.4 Feed mechanism

3.4.1 Background

As noted in the previous chapter, the design of the feed mechanism forms the most critical part of the antenna design as it essentially determines the bandwidth of the antenna. The different methods of accomplishing this were also discussed. In this section,

the design of a stripline-slotline transition as a feed mechanism is described. This design has been implemented based on the parametric study performed by Schaubert and Shin^[25], which basically makes use of the stripline-slotline feed mechanism. The microstrip-slotline transition has a lot of advantages over the other mechanisms. This transition can be easily fabricated by normal photo-etching processes. Also, two-sided circuit boards are possible with the microstrip on one side and the slotline on the other. Moreover, the authors have parameterized the antenna and hence the design is a lot easier to fabricate than the other designs. All these factors helped me in deciding the type of feed mechanism for the antenna.

3.4.2 Stripline-slotline transition

A detailed introduction to the microstrip/stripline-slotline transition has been done in the previous chapter. The issues pertaining to the actual design of this transition will be discussed in this section. As the name suggests, the microstripline/microstrip-to-slotline transition (Figure 3.2) basically consists of,

- Stripline, used as a connection to the transmitter/receiver circuitry.
- Slotline, which is flared outwards from the feed.

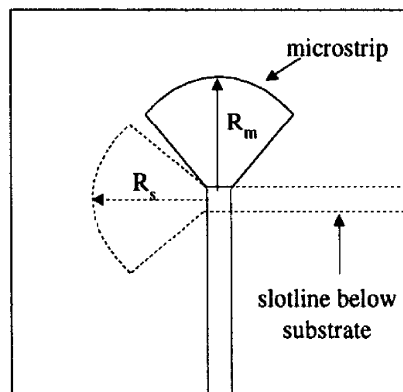


Figure 3-2: Microstrip-slotline transition

Previously, transitions were reported with both straight uniform stubs as well as non-uniform circular ones. The radial stub was used here which eliminated the problem of overlapping of the stubs and also provided a better bandwidth than the other two. The microstrip-to-slotline transition design was adapted from the design by Sloan et al. [20]. As previously discussed, the stubs extend a quarter-wavelength further from the crossing point. Due to this quarter-wavelength transformation at the overlap, the stripline open circuit stub appears as a short circuit while the slotline short circuit appears as an open circuit at the crossing reference plane. Designing a good quarter-wavelength stub is crucial to obtain a fairly wideband transition.

3.4.3.1 Stripline design

According to the parameter study [25], using stripline and slotline widths of 1mm, a wideband (1 – 5+ GHz) Vivaldi antenna with a 0.288 cm thick substrate was predicted. Hence I decided to design the stripline feed with a width of 1mm. The stripline triplate structure is shown in the Figure 3.3 with the different variables listed in Table 3.2.

Feature	Value
Substrate thickness, b	2*0.1575 cm
r	2.22
Conductor thickness, t	
Strip width, w	1 mm

Table 3-2: Stripline parameters

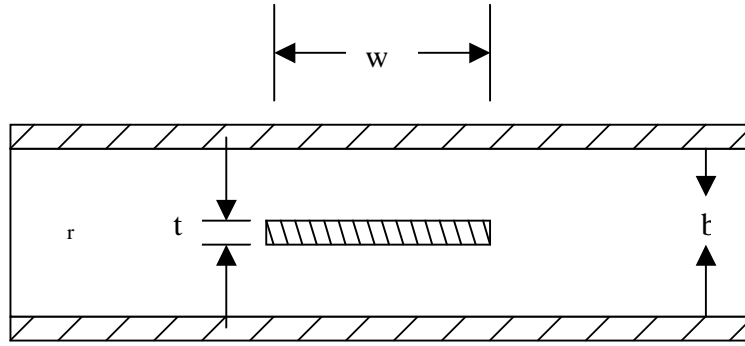


Figure 3-3: Stripline Triplate Structure

Based on the formula given in Wadell^[28] (Eqn 3.1) and using LineCalcTM routine in ADS EESof^[R]

the conductor thickness was neglected, the characteristic impedance was obtained as

Ansoft HFSS^[R]

agrees well with the calculated value.

$$Z_0 = \frac{\eta_0}{2.0\pi\sqrt{\epsilon_r}} \ln \left\{ 1.0 + 0.5 \frac{8.0b}{\pi w'} \left[\frac{8.0b}{\pi w'} + \sqrt{\left(\frac{8.0b}{\pi w'} \right)^2 + 6.27} \right] \right\}$$

$$2.0h = b$$

$$w' = w + \frac{\Delta w}{t} t$$

$$\frac{\Delta w}{t} = \frac{\ln\left(\frac{5.0b}{t}\right)}{3.2}$$

Here,

'b': Thickness of the stripline substrate; 't': Thickness of conductor; 'w': Stripline width;

η_0 : Characteristic impedance of the stripline.

The stripline open circuit stub was chosen to be of length 8 mm as specified in the paper [25]. It was shown that stripline radial stub reactance varied from large capacitive values at the lower frequencies through a near-zero reactance in the mid-band region to inductive values in the upper band^[25].

This behavior of the stub reactance results in favorable compensation of the antenna reactance, contributing to the wideband performance. The use of the radial/circular stubs have been shown to achieve a significantly better bandwidth than the uniform stubs [18], [20]. Moreover, designing non-uniform stubs is easier with modern etching processes.

3.4.3.2 Slotline design

The slotline plane of the antenna consists of the circular slotline cavity, the uniform slotline input and the tapered radiating slot. The general configuration of a slotline is shown in Figure 3.4.

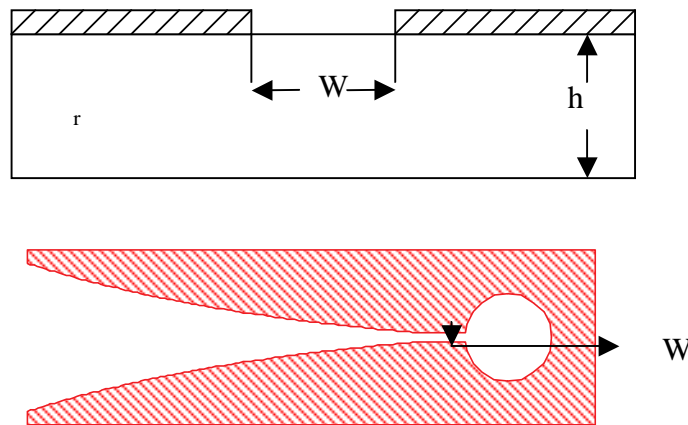


Figure 3-4: Slotline structure – end and top views

The slotline width at the transition region was chosen to be 1 mm. As reported by Schaubert, this transition setup worked well in a frequency range between 1 GHz and 5

GHz [25]. The slotline wavelength and the characteristic impedance were calculated using formulae given in [15].

The formulae specified are empirical and not in any case exact. The center frequency of 5 GHz is chosen for all the calculations with the substrate parameters being the same as

s was found to be 5.2 cm and the

$$2.22 \leq \epsilon_r \leq 9.8$$

$$0.0015 \leq W/\lambda_0 \leq 1.0$$

$$0.006 \leq h/\lambda_0 \leq 0.06$$

$$\lambda_s/\lambda_0 = 1.045 - 0.365 \ln \epsilon_r + \frac{6.3(W/h)\epsilon_r^{0.945}}{(238 + 100W/h)} - \left[0.148 - \frac{8.81(\epsilon_r + 0.95)}{100\epsilon_r} \right] \bullet \ln\left(\frac{h}{\lambda_0}\right) \dots\dots(Eqn.3.2)$$

$$Z_{0s} = 60 + 3.69 \sin\left[\frac{(\epsilon_r - 2.22)\pi}{2.36}\right] + 133.5 \ln(10\epsilon_r) \sqrt{W/\lambda_0}$$

$$+ 2.81[1 - 0.01\epsilon_r(4.48 + \ln \epsilon_r)](W/h) \ln\left(100h/\lambda_0\right)$$

$$+ 131.1(1.028 - \ln \epsilon_r) \sqrt{h/\lambda_0} + 12.48(1 + 0.18 \ln \epsilon_r) \frac{(W/h)}{\sqrt{\epsilon_r - 2.06 + 0.85(W/h)^2}}$$

Based on [25], I chose the slotline cavity diameter as 1 cm with a uniform slotline extension of 5 mm. It was shown that increasing the size of the cavity decreased the lowest frequency of operation of the antenna (when in an array) thus essentially widening the bandwidth.

To test the frequency response of the transition, two transitions were cascaded together on a RT/Duroid 5880 substrate. This setup was then modeled in Ansoft HFSS^[R] using the same substrate material, substrate and conductor thickness as mentioned in Table 3.2.

The model is shown in Figure 3.5. H-plane symmetry has been used and hence only half of the model has been modeled to save memory and simulation time.

Design Feature	Value
Substrate	RT/Duroid ^[R] 5880
Height	2*0.062"
Stripline width	1 mm
Slotline width at cross plane	1 mm
Stripline stub length	8 mm
Slotline cavity length	10 mm
Length of uniform slotline	3.4 cm

Table 3-3: Transition parameters

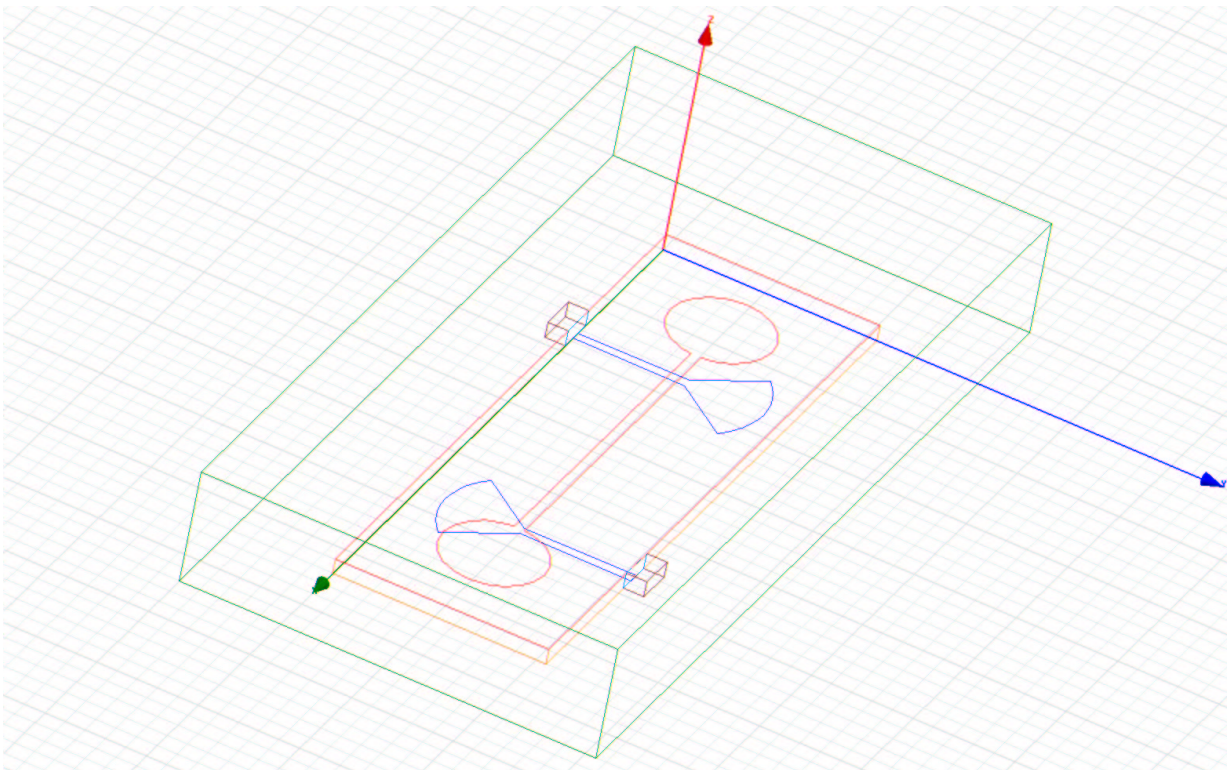
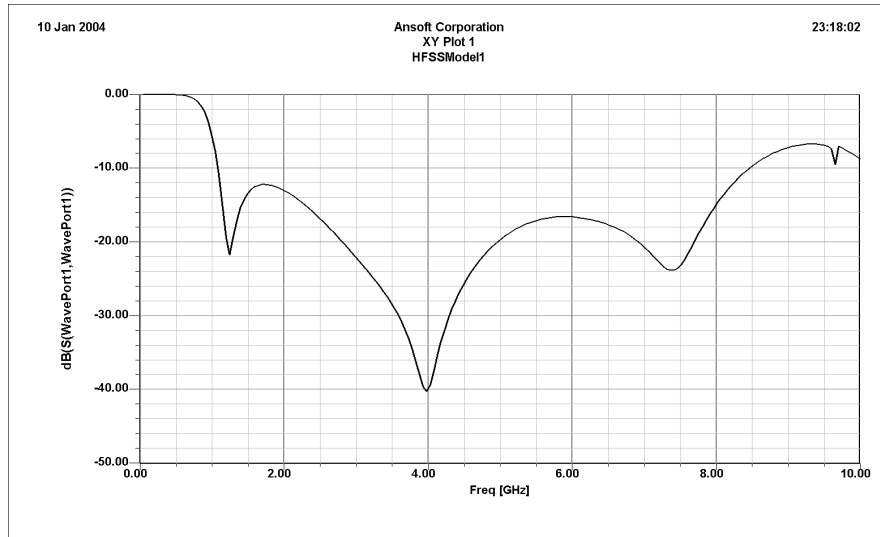


Figure 3-5: Double transition in HFSS^[R]

The S11 and S21 results (Figure 3-6) shown that this transition is wideband with the S11 less than -10 dB throughout the required bandwidth of 2-8 GHz. Also, the S21 is greater than -3 dB in the same frequency range. These results proved that the transition as proposed by Schaubert could also be used in the frequency range of interest.



(a)

(b)

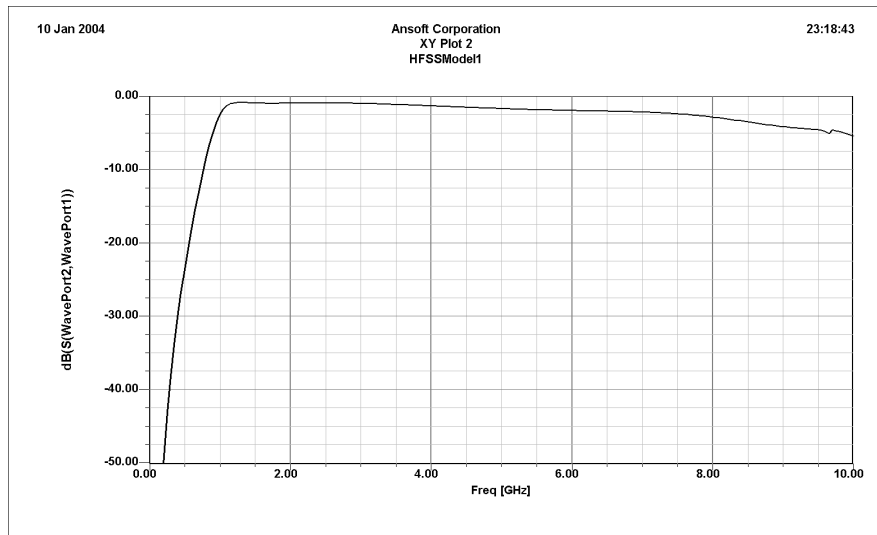


Figure 3-6: (a) S11; (b) S21 - Simulation results of the transition

3.5 Taper design

As discussed in the previous chapter, the TSA with an exponential taper is referred to as the Vivaldi antenna. Numerous exponentials have been used in the literature^{[3], [18], [20], [25]}. Schaubert, in his design, has used the following exponential relations to design the taper. With reference to Figure 3-7, R is defined as the opening rate and the points P₁(z₁,y₁) and P₂(z₂,y₂) are the two end points of the taper profile. A closer look will reveal that P₁ is actually the point where the slotline starts to flare after a short of uniform line from the cavity. The difference z₂ – z₁ is the flare length L, as shown in the picture below. It is worth mentioning that when R becomes zero, the slope of the taper becomes constant resulting in a linearly tapered profile, commonly referred to as the LTSA.

$$y = c_1 e^{Rz} + c_2$$

where

$$c_1 = \frac{y_2 - y_1}{e^{Rz_2} - e^{Rz_1}}$$

$$c_2 = \frac{y_1 e^{Rz_2} - y_2 e^{Rz_1}}{e^{Rz_2} - e^{Rz_1}}$$

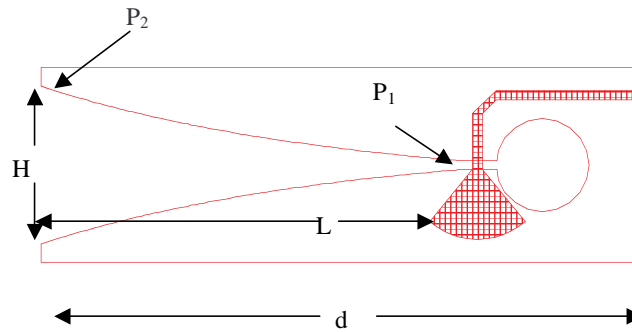


Figure 3-7: Vivaldi antenna parameters

A taper length L of 4.5 cm and an aperture height H of 1.7 cm were chosen for this design based on the parameter study. As the length of the taper is increased, for the same

aperture height, the flare angle is reduced correspondingly. It was reported [25] that for small flare angles, the lowest operating frequency of the array reduces and subsequently the bandwidth increases. Similar study was also done for the opening rate R of the exponential flare. For larger opening rates, the flare angle becomes small at the origin and the lowest frequency of operation reduces as before. Further increase produces significant improvement in the SWR at the higher operating frequencies. A value of 0.3 was finally chosen for R based on the data given in [25]. All these values were chosen based on the plots given in the referred publication by comparing the VSWR and antenna resistance characteristics.

3.6 Array design

3.6.1 Introduction

The single element Vivaldi antenna is unmatched throughout the bandwidth. Due to this mismatch, there is too much reflection from the antenna and the antenna becomes unusable. Another major drawback of this single element configuration is that it is characterized by a fairly low gain across both planes of radiation which hampers our objective. As explained earlier, going for an array configuration would help in building smaller antenna elements rather than realizing large single antennas.

Radiation pattern of an array is determined by the type of the individual element used, their orientations, their positions in space, and the amplitude and phase of the currents feeding them^[30]. The basic array pattern consists of two parts, the pattern of one of the elements by itself which is aptly called the element pattern and the pattern of the array with the actual elements replaced by isotropic sources, referred to as the array factor. The

total pattern of the array is then the product of the element pattern and the array factor. The procedure just explained is often referred to as pattern multiplication.

3.6.2 Array factor

The basic configuration of an array antenna is the linear array. As the name suggests, it is an arrangement of the antenna elements in a single straight line with the appropriate feed network and phase shifters, if needed. To determine the array factor, the elements are assumed to be point sources that radiate equally in all directions, commonly known as isotropic radiators, but retaining their respective locations, their input feeds and phase differences in them, if any. The distance of separation between the elements is very crucial in the proper design of the array. This distance dictates the phase difference between the elements and is inherent to the array.

It is really intuitive to arrive at the array factor for a small linear array, given its setup and input feed characteristics by what is called the inspection method. Consider a linear array of two ele

and no additional phase shifting given on the inputs. At the far-field of the antennas, the waves arriving from the elements on an axis perpendicular to the line joining the two sources, add in phase and hence we would see a field maximum in that region. On the other hand, along the axis of the array, the waves cancel each other at the far-field due to the phase difference created by the separation between the two sources. A picture of the two element linear array just described and its array factor is shown in Figure 3-9. The polar plot would reveal what was described earlier in this paragraph.

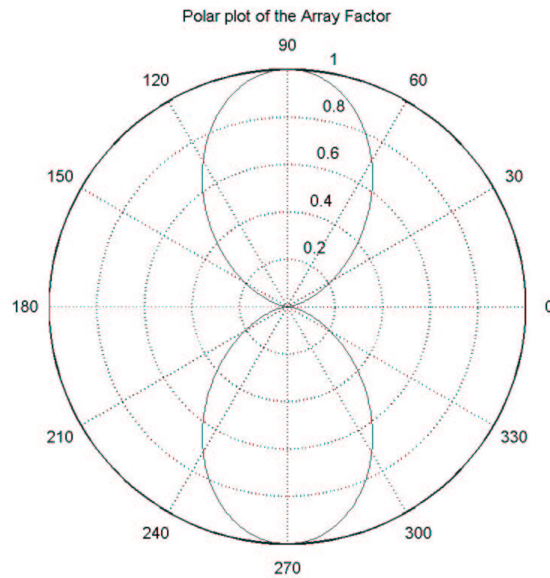


Figure 3-8: AF of 2 isotropic sources with identical amplitude and phase currents spaced one-half wavelength apart

3.6.3 Mutual Coupling

The inspection method, though intuitive cannot be used for more complex arrays with more number of elements and complex phase differences and distance of separation. Moreover, all these derivations have been based on the assumption that all the elements are isolated from each other and from external sources. However, in practice, this is rarely the case. Each element interacts with all the other elements in the array creating what is known as the mutual coupling which causes changes in the current magnitude, phase, and distribution on each element. The end result is that the total array pattern is different from the no-coupling case.

Mutual coupling not only depends on the proximity of the elements, but also on the frequency and scan direction. Also, it was found that mutual coupling decreases as the

spacing between elements increases and that the coupling strength is predicted by the far-field pattern of each of the elements. The input impedance of the ‘ m ’th element in the presence of all other elements and with mutual coupling included is expressed as^[26],

$$Z_m = \frac{V_m}{I_m} = Z_{m1} \frac{I_1}{I_m} + Z_{m2} \frac{I_2}{I_m} + \dots + Z_{mN} \frac{I_N}{I_m}$$

This is referred to as the driving-point impedance. It is evident that input impedance of each element depends on the mutual impedances with the other elements in the array and the terminal currents.

3.6.4 Linear Vivaldi array

As discussed earlier, the inspection method would be easy to work with only for the simplest of linear array configurations. Hence, a Matlab^[R] code written by [31] was used to plot out the array factor for arbitrary linear arrays. It was observed that the array factor is a pattern that has rotational symmetry about the line of the array. Hence, its complete structure is determi

element spacing is one-half wavelength, exactly one period of the array factor appears in the visible region. The dimensions of the Vivaldi single element would make this impossible for us to achieve. Less than one period is visible when the spacing is less than

element phasings. Any other lobe equal in intensity to the major lobe is referred to as a grating lobe and its presence is undesirable.

In the case of the Vivaldi array, a linear configuration of twelve (12) elements was chosen. The next logical step was to decide the element spacing. In this specific

application, where the antenna was either going to be mounted underneath an helicopter, the vertical distance was expected to go up to 500 ft. Taking note of this, different array spacings were experimented in Matlab^[R]

the highest frequency (3.1875 cm at 8GHz) would satisfy our requirements. The grating lobes are about 100° away from the endfire main lobe and hence would be of no impact in any measurements taken in the nadir direction. The polar plot of the array factor for a 12 element array at 2 and 8 GHz are shown.

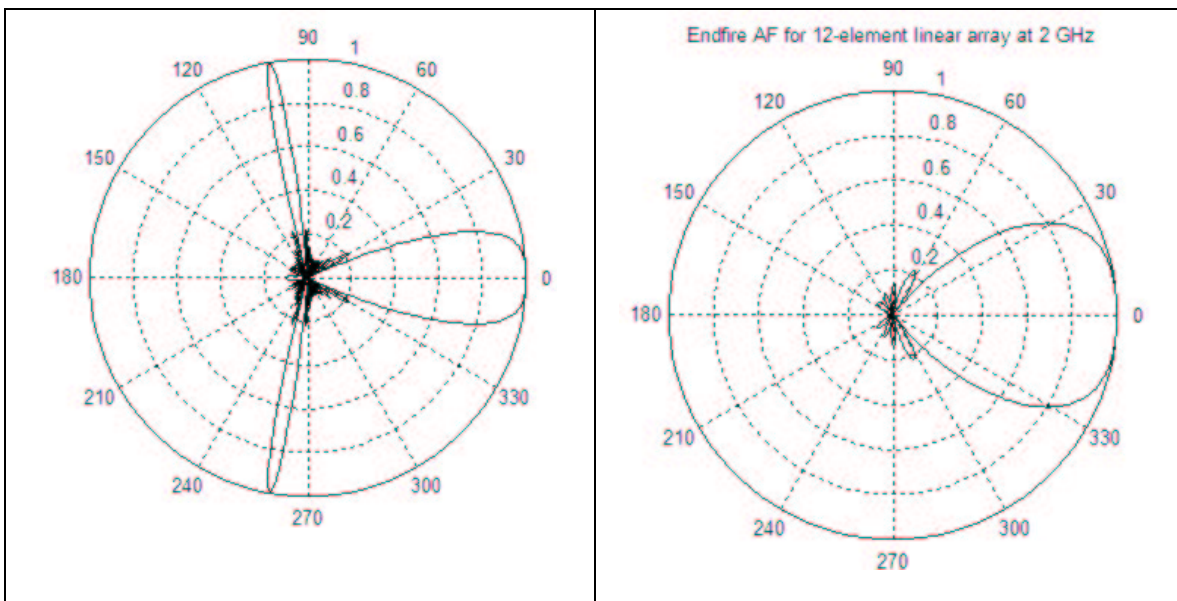


Figure 3-9: AF of an endfire 12-element linear array at 8 and 2 GHz

It is highly imperative to note that t -element spacing is calculated for the signal at the highest frequency of interest which is 8 GHz. This subsequently gives a distance of 3.1875 cm. But this distance would of course correspond to an entirely different relation at any other frequency and at the lowest frequency (2 GHz) its value is the pattern at 8 GHz. However, in any antenna design with such a high bandwidth, this discrepancy is bound to occur and hence striking a good engineering compromise

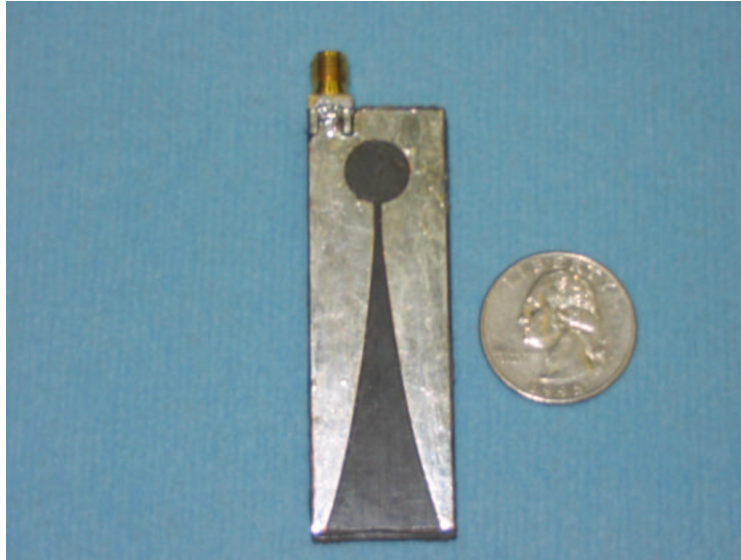
essentially becomes the catch. This compromise would again differ, based on the application for which the antenna is being designed. For our application, the value of $\lambda/4$ turned out to be a good choice, since the grating lobes were more than 90° away from the main end-fire lobe and hence it was decided to have it as the inter-element spacing in the 12-element array.

3.7 Fabrication

The Vivaldi antenna was fabricated as a stripline-fed triplate structure using the LPK Protomat[®] milling machine in the Remote Sensing Lab at the ITTC. The input feed to the stripline was accomplished by an SMA edge connector to realize a coaxial input. The outer ground pins of the SMA receptacle were shorted to the slotline ground planes of the antenna. The center pin of the SMA was then soldered to the stripline transmission line. A wedge/notch had to be made on the copper-less face of one of the dielectrics so that the center pin of the SMA sits in between the two boards with no air-gaps. Since it was a triplate structure, the two 0.062" RT/Duroid[™] 5880 boards had to be bonded together at very high temperatures of the order of 220°C with the special-purpose Rogers 3001 bonding film. A similar procedure was followed for fabricating the array antenna.

One major addition that was done to the array antenna was the back ground plane. The application required that most radiation be oriented in the direction along the flared slot. The purpose of the backplane, which was made of metal, was to reflect any radiation going in a direction opposite to that of the required. This would then effectively increase the forward radiation thus contributing to the gain of the antenna structure.

A picture of the single-element Vivaldi antenna as well as the twelve-element linear array is shown in the below.



(a)

(b)

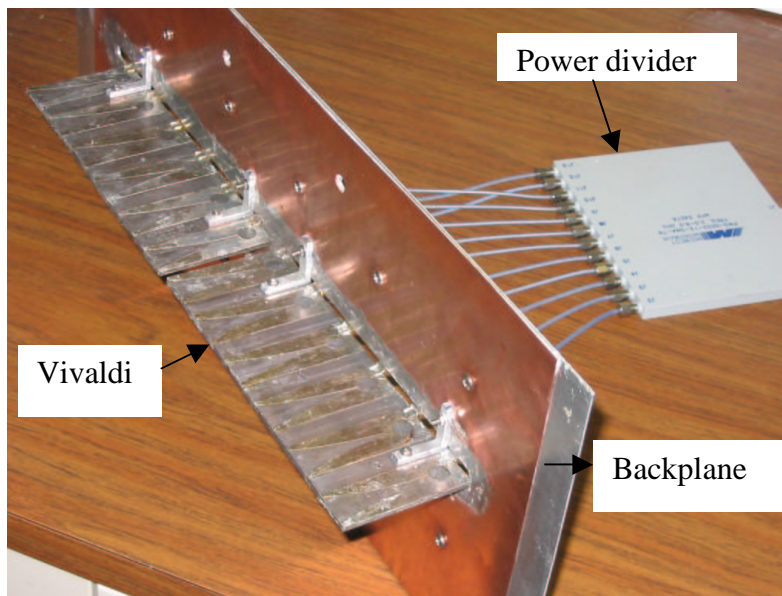


Figure 3-10: (a) Single element Vivaldi antenna; (b) 12-element Vivaldi array

3.8 Summary

The most crucial aspect of the design of the Vivaldi antenna – the feed mechanism, was designed and simulated using Ansoft HFSS and then incorporated into the antenna

design. The transition was found to be of very wide bandwidth. The input impedance of design like the taper width, opening rate, flare angle, size of slotline cavity as discussed by [25] were considered and based on the reported performance, the nominal values were chosen. The S11 was measured and the results are shown in Chapter 5 of this report. The 12-element Vivaldi array antenna was then designed with an inter-element spacing of best frequency (8 GHz) which turned out to be 3.1875 cm. The metal backplane was then added to the array so that any signal going in the backward direction would be reflected. The design features are summarized in the table below.

Feature	Description/Value
Material	ϵ_r 2.22, 2*0.062" thick
Antenna length	6.4 cm
Antenna width	2.1 cm
Aperture height	1.7 cm
Taper length	4.5 cm
Opening rate	0.3
Stripline & slotline input width	0.1 cm
Backwall offset	0.5 cm
Array spacings	λ 8 GHz

Table 3-4: Antenna features

Chapter 4 Simulation

4.1 Introduction

Antenna designs, however efficient they might be, could be understood a lot better when their performance is simulated. Generally in antenna problems, the actual practical result might not be the same as the one predicted by theory and a better understanding of the functionality of the structure in terms of the reflection and radiation characteristics is warranted. In this project, the High Frequency Structure Simulator (HFSS) of Ansoft has been used extensively to perform antenna simulations.

Ansoft HFSS is an interactive software package for calculating the electromagnetic behavior of a structure. The software also includes post-processing commands for analyzing the electromagnetic behavior of a structure in more detail. Using Ansoft HFSS, one can compute:

- Basic electromagnetic field quantities and, for open boundary problems, radiated near and far fields.
- Characteristic port impedances and propagation constants.
- Generalized S-parameters and S-parameters renormalized to specific port impedances.

The task at hand for the antenna designer is to first draw the structure, specify material characteristics for each object and identify ports and special surface characteristics. The system then generates the necessary field solutions and associated port characteristics and S-parameters. As we set up the problem, Ansoft HFSS allows us to specify whether to solve the problem at one specific frequency or at several frequencies within a range. We

may choose to perform a fast frequency sweep that generates a unique full-field solution for each division within a frequency range, a discrete frequency sweep that generates field solutions at specific frequency points in a frequency range, or an interpolating frequency sweep that estimates a solution for an entire frequency range.

This chapter describes the simulations that were performed on the different antenna configurations with HFSS. The following section describes the different setups that were simulated and presents and discusses the results of the S-parameter and field plots. Antenna parameters like the peak gain, peak directivity, etc could also be calculated using HFSS and are displayed at appropriate places.

4.2 Description

A number of simulations were done in HFSS with a variety of Vivaldi antenna configurations. Considering their relevance to the final result only a few of them are going to be discussed here in this section. The different designs that will be discussed are listed below.

- The single element stripline-fed triplate-structured Vivaldi antenna.
- The Vivaldi infinite array with a backplane (ground) which could then be approximated for a finite array configuration.

All the different designs are modeled based on the same principles. The common features of the design are listed below and further modifications are explained in the respective sections. Each design is described with the help of plots, figures and parameter values generated after the simulation. Table 4-1 lists the general settings that were used in the simulation.

Feature	Setting
Symmetry	H-plane (only half of the actual structure is modeled)
Stripline/Slotline	Perfect E
Radiation absorber	Perfectly Matched Layers (PMLs), at typical
Port	Waveport (integration line defined)
Orientation	XY plane with maximum radiation towards negative X-direction
Adaptive Freq.	At 6 GHz, typically with 10-15 passes for the mesh to converge
Sweep	2-8 GHz interpolating sweep with 201 points
E plane; H plane	
Outputs	S-parameters, port Z_0 , pattern cuts, half-power beamwidth (HPBW)

Table 4-1: General simulation settings in HFSS

4.2.1 Single element Vivaldi antenna

The basic setup of the antenna is shown below.

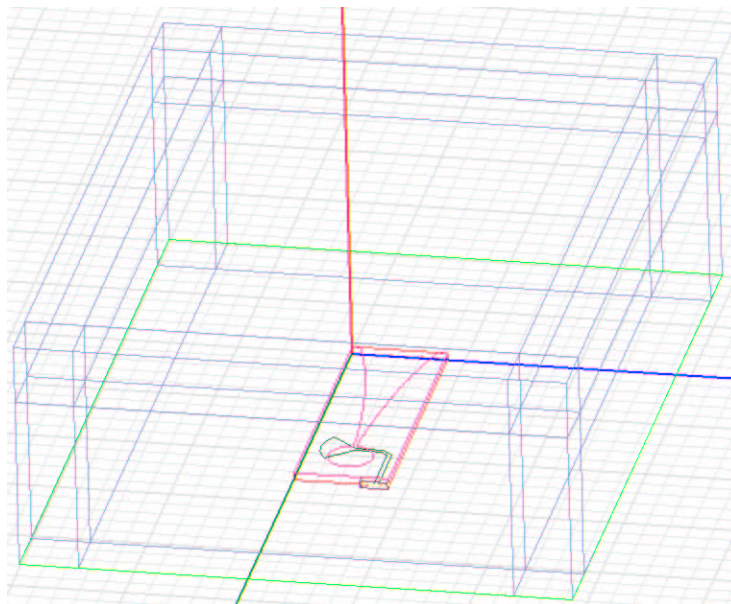


Figure 4-1: Single element Vivaldi model

The S11 looking into the input port of this antenna is shown below. It is obvious that the antenna has a very poor match for frequencies less than 7 GHz. The characteristic impedance was found to be

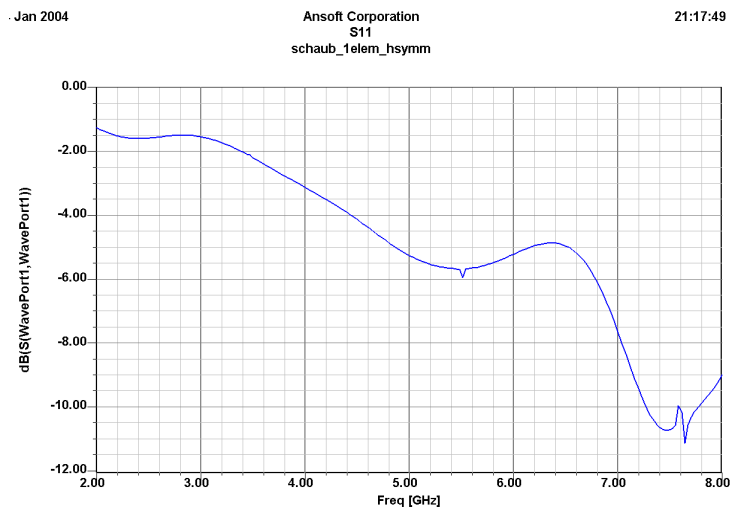


Figure 4-2: S11 of single element Vivaldi antenna

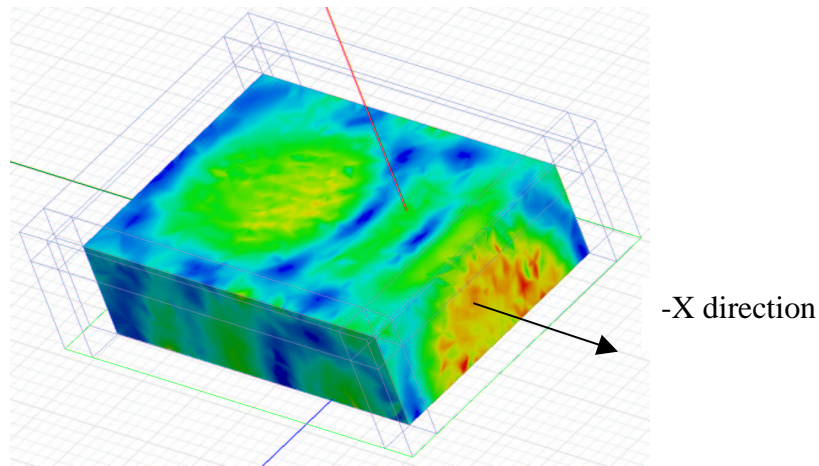


Figure 4-3: E-field plot of structure

Figure 4-3 shows the E-field plot of the antenna structure with red being the highest in the intensity scale and blue the lowest. From the plot it is clear that the maximum

radiation intensity (in red hue) in on the negative-x direction or in other words, the antenna exhibits endfire radiation.

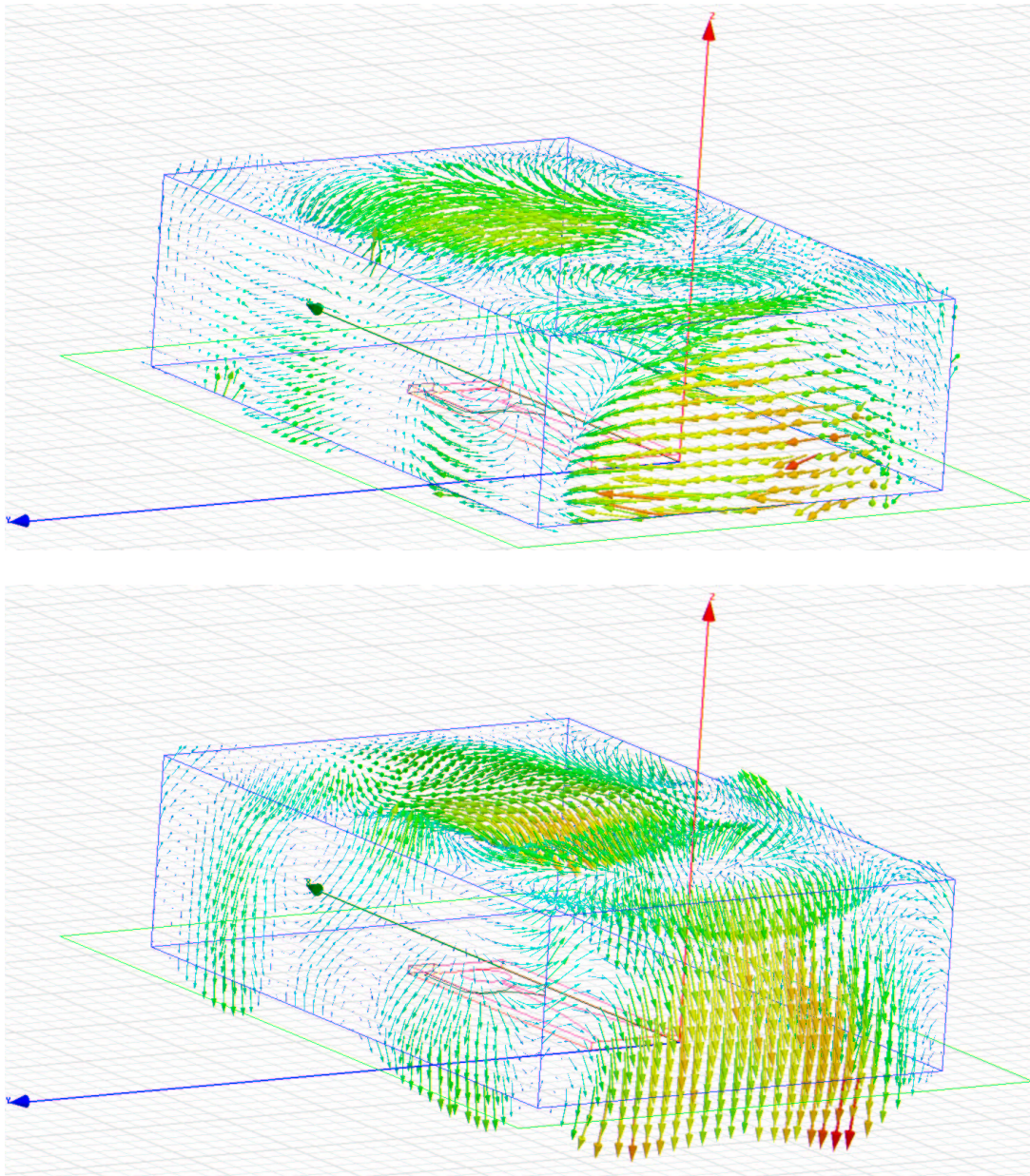


Figure 4-4: E & H field intensity vectors

From the plots shown above, the orientation of the E and H field vectors becomes clear. Considering the principal direction of radiation (main lobe) in both cases, the E/H-plane is the plane containing the E/H-vector and passing through the origin. Thus the XY plane is the E-plane while the XZ plane is the H-plane.

The E-plane and H-plane cuts for the frequencies of 2, 4, 6 and 8 GHz are shown below. The plots shown below are for the total absolute gain of the antenna at the above mentioned frequencies. It is seen that the gain is clearly a function of frequency and that the pattern is definitely a smooth one as it has a couple of sidelobes.

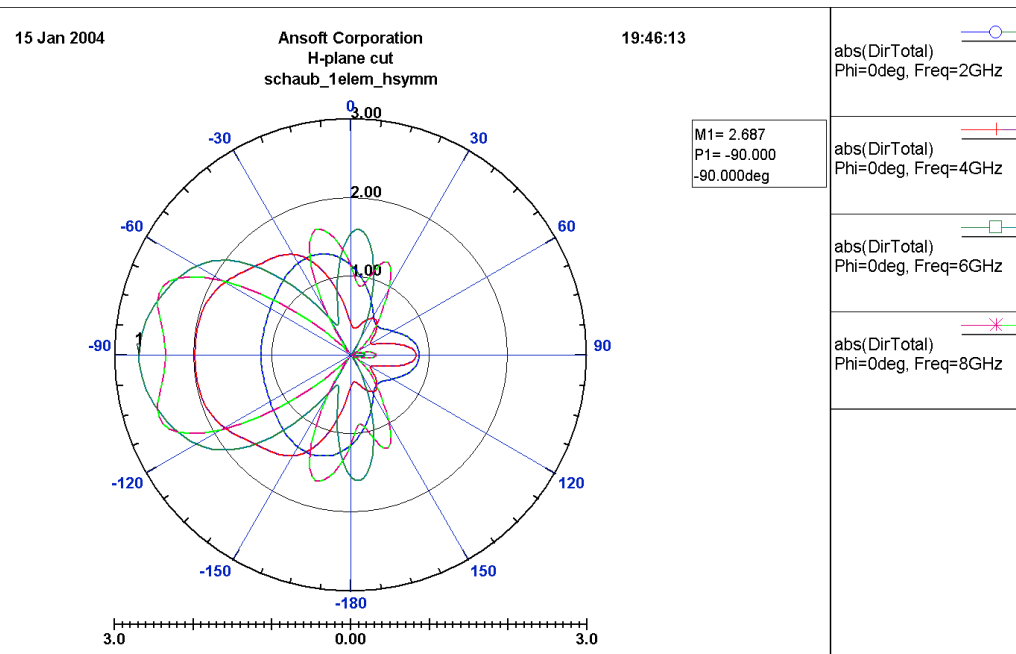
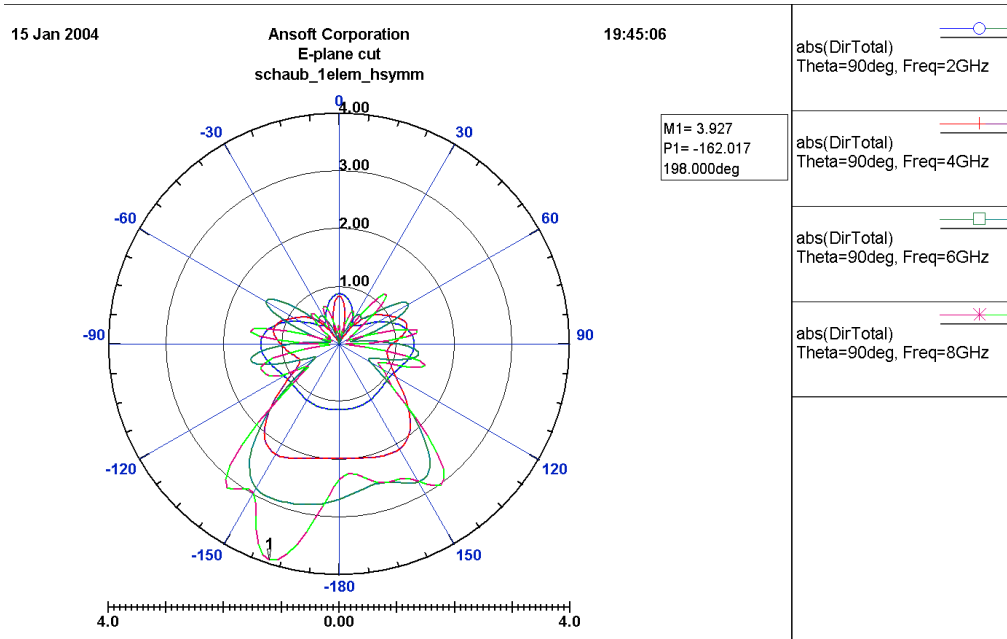


Figure 4-5: E & H plane cuts of Vivaldi antenna

The Half-Power Beam Width (HPBW) is plotted in the figure below in both the H and E planes. This plot along with the polar plots shown in the previous page show that the Vivaldi is an end-fire radiating type of antenna. This further agrees with the theory as

discussed in the literature. It is also seen that the peak gain on the E-plane (3.927) is only slightly greater than that of the H-plane (2.687).

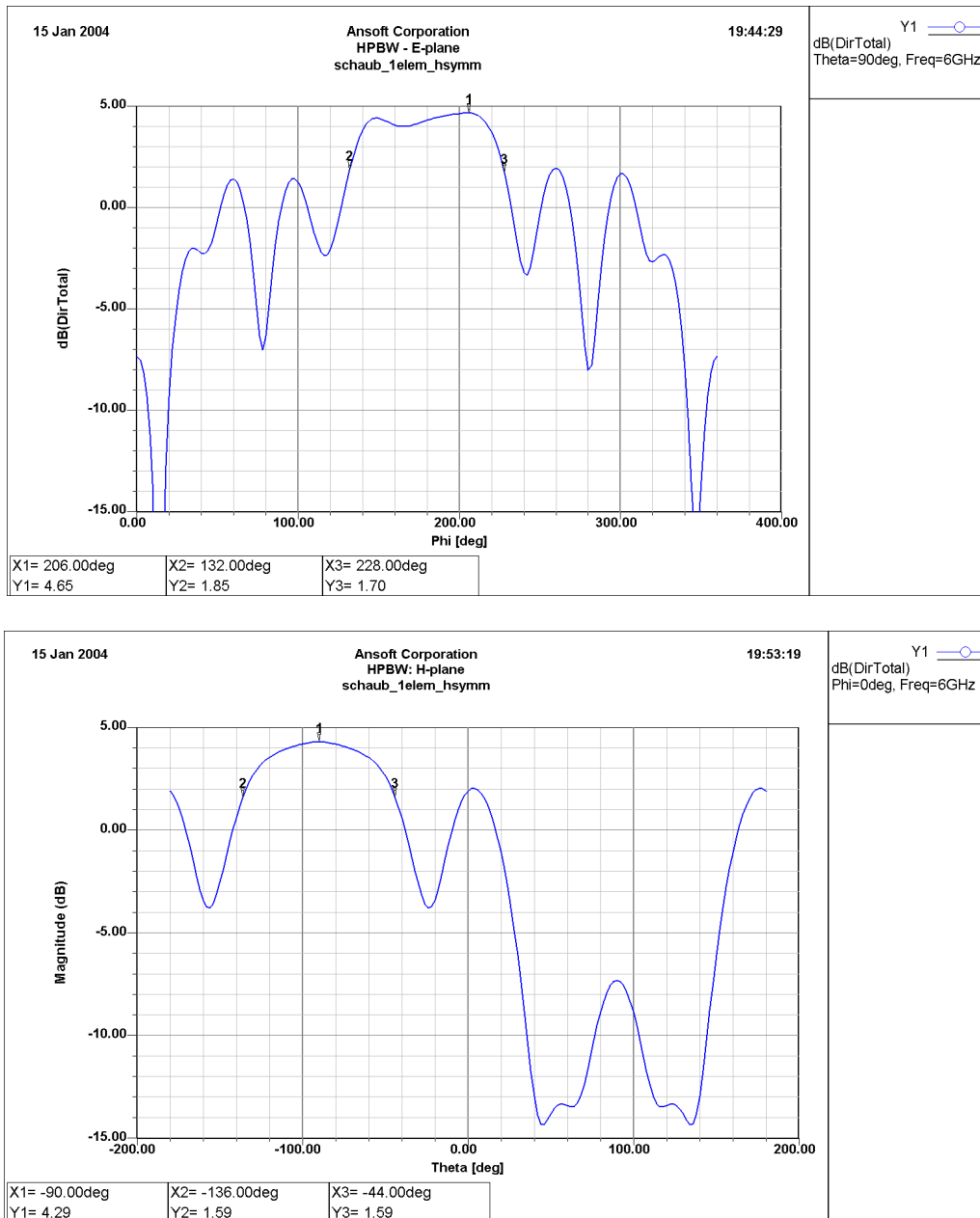


Figure 4-6: E & H plane rectangular plots

The antenna parameters that typically describe any antenna are listed below. The parameters are for a signal frequency of 6 GHz which was frequency at which the

software created its mesh. The HPBW in both the H and E planes are exactly same, as predicted by Gibson [5]. The radiation efficiency of 0.98 obtained is particularly very good. This concludes the single-element simulation of the Vivaldi antenna.

Antenna Parameter (6 GHz)	Value
Max. radiation intensity, U_{\max}	0.158 W/Sr
Peak directivity	2.9
Peak gain	2.84
Realized gain	1.98
Radiated power	0.68 W
Accepted power	0.7 W
Input power	1.0 W
Radiation efficiency	0.98
HPBW (E-plane)	96°
HPBW (H-plane)	96°

Table 4-2: Antenna parameters at 6 GHz

4.2.2 Infinite Vivaldi array with backplane

Once the single element simulation is completed, the next step was to try and simulate the antenna in the array configuration. Ideally, we would like to simulate an array with twelve elements so that the measurements could be compared with the simulation. However, simulating 12 elements in HFSS at the frequency of our interest was highly difficult as the memory requirements exceeded even the most powerful computer in the lab. For the sake understanding, the single element simulation sweep took almost a day to

get over. To circumvent this problem, the concept of infinite array simulation using periodic boundary conditions was used in HFSS.

In this method, the model is setup similar to the single-element simulation. To be precise, just one element is modeled in the design layout. The only difference between the two is that the sides of the model which lie (or expect to) on the axis of the array, are defined Linked Boundary Conditions (LBCs). The heart of the simulation is the setting up of the two types of LBCs in the model, namely the master and slave boundaries. These enable one to model planes of periodicity where the E-field on one surface matches the E-field on another to within a phase difference. In other words, the LBCs force the E-field at each point on the slave boundary to match the E-field to within a phase difference at each corresponding point on the master boundary.

These boundaries are also called periodic boundary conditions. The advantage of using these is that by modeling just a single element, the pattern for an infinite array could be determined. All the effects of mutual coupling are also included with this setup. Once the simulation is done, the user could then define an array of arbitrary size and the pattern specific for that configuration could then be obtained.

It is important to note that the realization of the antenna characteristics with the custom array setup is just an approximation that is arrived from the infinite array model. This approximation gives good results if the array size is huge. For relatively small arrays, like the one designed in this project with 12 elements, the approximation might become erroneous or in some invalid. However, this configuration was attempted just to verify how the pattern looks like and to get a rough estimate of the gain of the 12 element array antenna.

A further addition to the original single element Vivaldi is the metal backplane. This feature was suggested by Schaubert [25] and was basically used to reflect any signal power going in the backward direction. This would then reduce the backlobe in the model, if not completely.

The infinite array was then modeled in HFSS with the new master-slave settings and the backplane with the other settings remaining the same. The model is shown below.

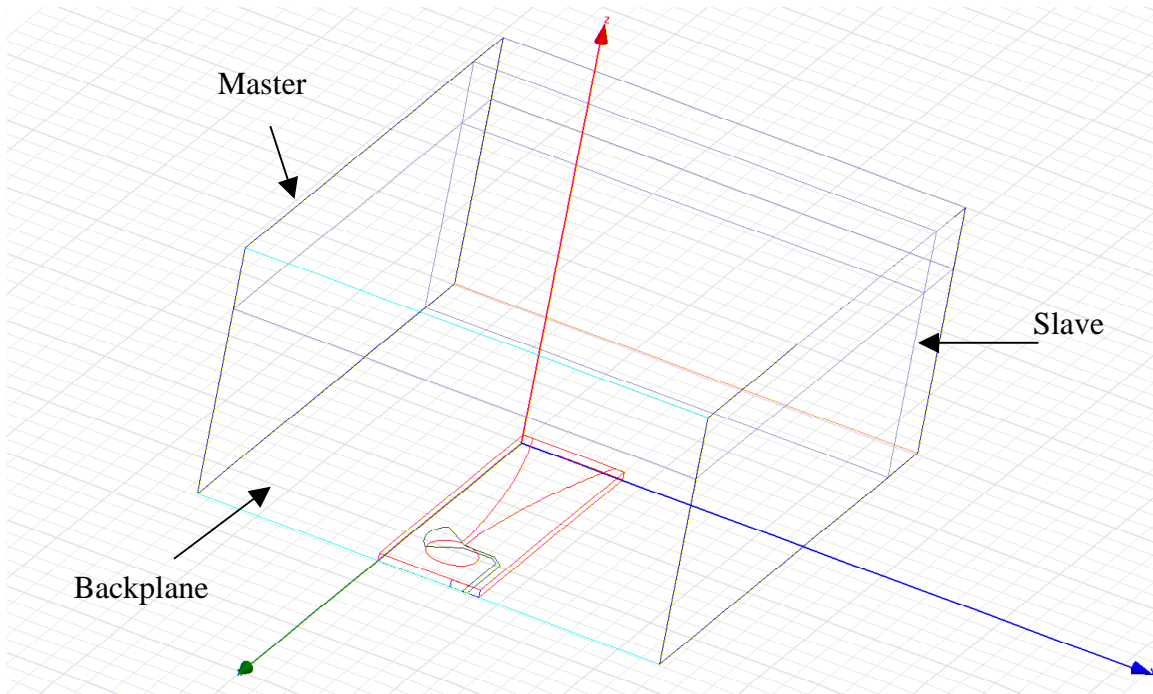


Figure 4-7: Infinite array Vivaldi model

The radiation pattern plots obtained from the 12 element array approximation are shown in the next page. As previously explained, this model is just a rough approximation and it has its own shortcomings. The driving-point impedance, as defined earlier, could not be determined for this configuration. For obtaining this value, a simulation with all the 12 elements should be carried out which the solver is not capable of doing even with the most powerful computer resources available in the lab.

The E and H field intensity vectors resemble that of the single element and are hence not shown to save space. The 3-D radiation pattern is shown below. At 6 GHz, it is seen that the main beam has become narrow in the E-plane and that is essentially due to the array configuration. In addition, two side lobes are seen in the pattern.

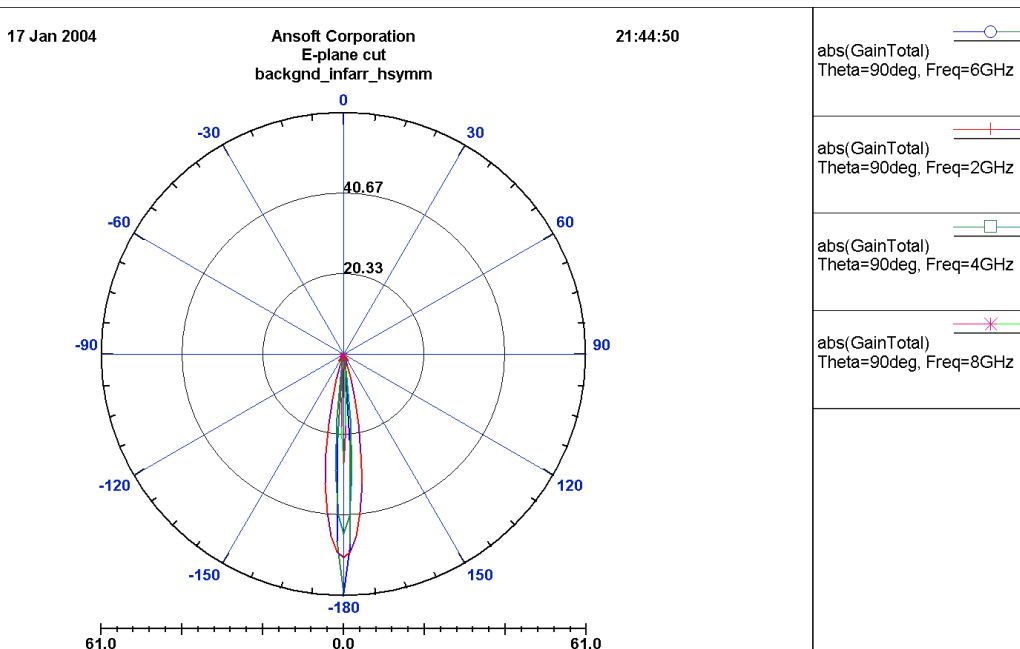
To revisit the discussion that we had in the previous chapter - It is well known that the element spacing in any array is very crucial in deciding its radiation characteristics. This is obvious at lower frequencies like 2 and 4 GHz. It must be noted that the spacing of

the lowest frequency 2 GHz. This enormous discrepancy results in a lot of variations in the resultant array beam pattern and the results are shown below in the 2-D field cuts. It is understood that this is a compromise that we would have to make in order to design an antenna with such a huge bandwidth.

The E-plane cut does not reveal much as the patterns look similar at the various frequencies. However, it is clear that the beamwidth in the E-plane is very narrow (of the order of degrees) which suggests the adding up of signals from the different elements of the array in that direction. This makes sense considering the configuration of the array.

The H-plane cut at different frequencies as shown in the next page. It is seen that as we go higher in frequency (from 2 to 8 GHz), the H-plane pattern becomes narrower and grating lobes begin to show up. For example, the pattern at 8 GHz breaks into two grating lobes, each at about 30° away and 3 dB above the lobe in the endfire direction, while the pattern at 2 GHz has a single broad beam.

The effect of the grating lobe on any measurements taken with the antennas could be understood better with the help of the following simple calculation based on trigonometry. The antenna was first assumed to be mounted at a height of 500 ft from the top of the snow surface and looking down. The principal direction of interest would then be the nadir direction and anything else would have to be removed. For a grating lobe 30° away from the nadir, the range to the ground would be about 577 ft. Therefore, any unwanted returns resulting from the grating lobe, referred to as off-angle clutter, would still be located about 77 ft. further from the signal return from the main nadir direction. Thus, for a maximum snow thickness of 20 ft. (say), this off-angle clutter would appear about 57 ft. away from the snow returns which should not affect the measurement in any way. Thus, even with a performance as bad as the one at 8 GHz, meaningful measurements could be made with the current setup.



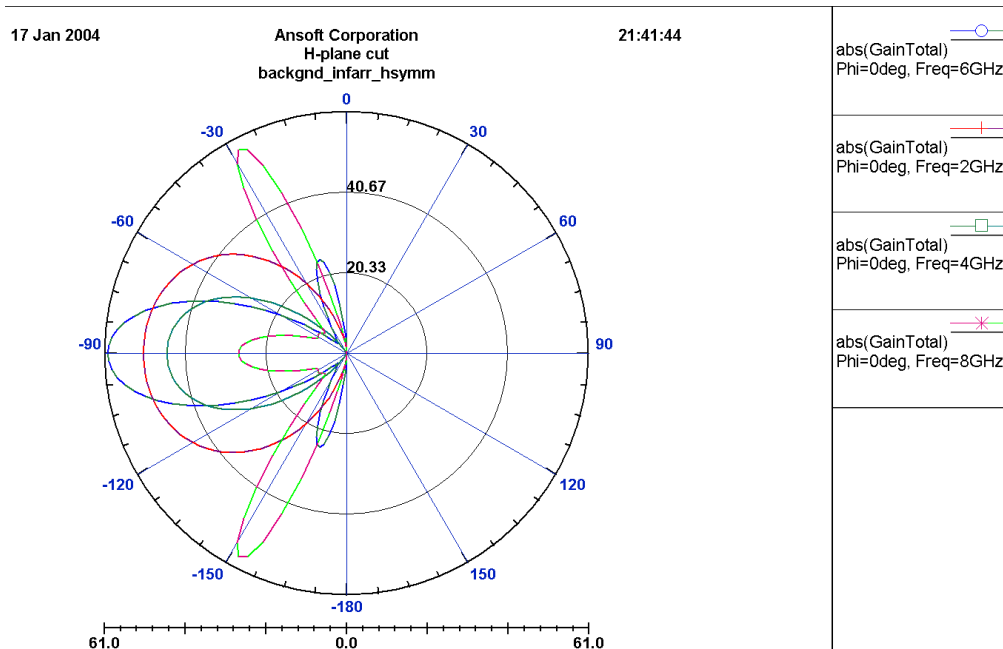


Figure 4-8: E and H plane cuts

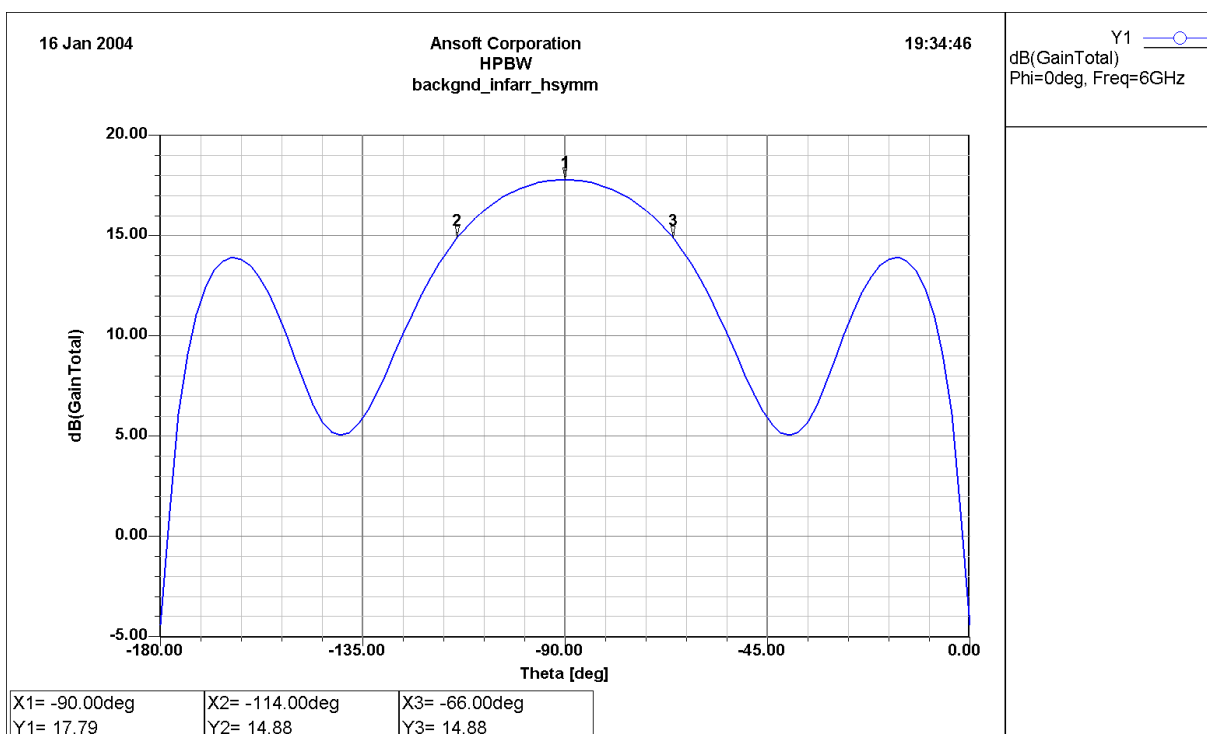


Figure 4-9: HPBW of 12 element linear array

The half-power beamwidth at 6 GHz was found out from the pattern plot on the rectangular scale shown above. It showed a total gain of 17.79 of about 48° . The twin grating lobes were about 4.5 dB down and 74° away from the main lobe. Assuming the same setup as earlier, with the antenna mounted about 500 ft. above the top snow surface, the signal return due to the grating lobe at 74° would be located at about 1800 feet. Again, for a maximum snow thickness of 20 ft., this off-angle clutter should not bring errors into the measurements.

This completes the simulation of the infinite array of Vivaldi elements. A look at the antenna parameters gave me a peak gain of about 60 and a realized gain of about 28. This means that if the antenna was perfectly matched at its input, a gain of about 60 is possible. The realized gain is the actual gain of the antenna after accounting for any loss due to mismatch at the port.

Thus, the pattern cuts have been studied for a 12-element array and they are found to vary as we go through the bandwidth of interest. Particularly, the pattern plots at 8 GHz revealed that two lobes of equal magnitude (grating lobes) at 30° away from the endfire direction. This could result in errors in the measurement when the antenna is used with the snow radar. The next task in hand is to cut the planes and measure the radiation pattern for the antenna array. This whole exercise was to just report the method of implementing the linked-boundary condition for simulating infinite arrays using HFSS. As explained earlier, it still remains a problem to simulate the full array due to computer resource issues.

Chapter 5 Test & Measurement

5.1 Background

Testing the antenna's characteristics forms one of the most important activities in the whole process. Moreover, of all the measurements that is made with any kind of circuit, the most difficult and least understood are those of antennas. This is because, in the case of circuits like filters, amplifiers, etc., enough accuracy can be achieved even with bench-top measurements. However, in the case of antennas, the surrounding environment plays a major role in deciding the accuracy of the tests being conducted and bench-top measurements are not feasible in most cases.

Generally, any antenna should be tested only in a place far removed from any objects that may cause spurious reflections, such that it is effectively in outer space. Since this is not possible under usual circumstances, at least a controlled environment is essential to make good antenna measurements^[32]. The most deleterious effect that any physical structure present in the test site would have on the measurement is that of multipath. This occurs when the signal bounces off from surrounding objects and interferes with the received signal from the direct path, resulting in a wrong measurement.

The following tests are typical of any antenna measurement setup.

- S-parameter, typically the reflection coefficient.
- Gain, with reference to an isotropic source
- Radiation pattern, both azimuth and elevation cuts.
- Polarization.

5.2 Power divider

One of the most important issues to be considered in any antenna test setup is the feed network. Each port of the twelve-element linear Vivaldi antenna has to be fed with the same input power level and phase offset. The antenna array can be driven from a single source by using a 1:12 power divider. We used a 12-way power divider from Midwest Microwave (Part # PWD-5522-12-SMA-79) for our feed network. This power divider was characterized by an insertion loss of 1.4 dB and an isolation of 15 dB over the frequency range 2-8 GHz. The data sheet of the power divider is attached in the Appendix.

The theoretical power split of a power divider depends on the number of splits accomplished in the divider. For an N-way power splitter, the power split would be $10 \log(N)$ dB, hence for a 12-way divider; the power split would then be 10.8 dB. The insertion loss of 1.4 dB that is specified in the datasheet is in addition to the theoretical power split of 10.8 dB. Hence the total insertion loss from the input port to any one of the output ports with the other ports matched would be $10.8 + 1.4 = 12.2$ dB. This component could be used both as a power divider as well as a combiner depending on the application.

The power divider was tested in the lab with the NA and the insertion loss and isolation characteristics were determined. It can be seen that the power divider works well in the lower frequency end while at the higher end; the insertion loss begins to increase. In fact, at 8 GHz, the measured insertion loss was about 14.5 dB, which was more than 2 dB higher than the loss specified by the manufacturers for the same frequency. The insertion loss and the isolation characteristic plots are shown in the figure below.

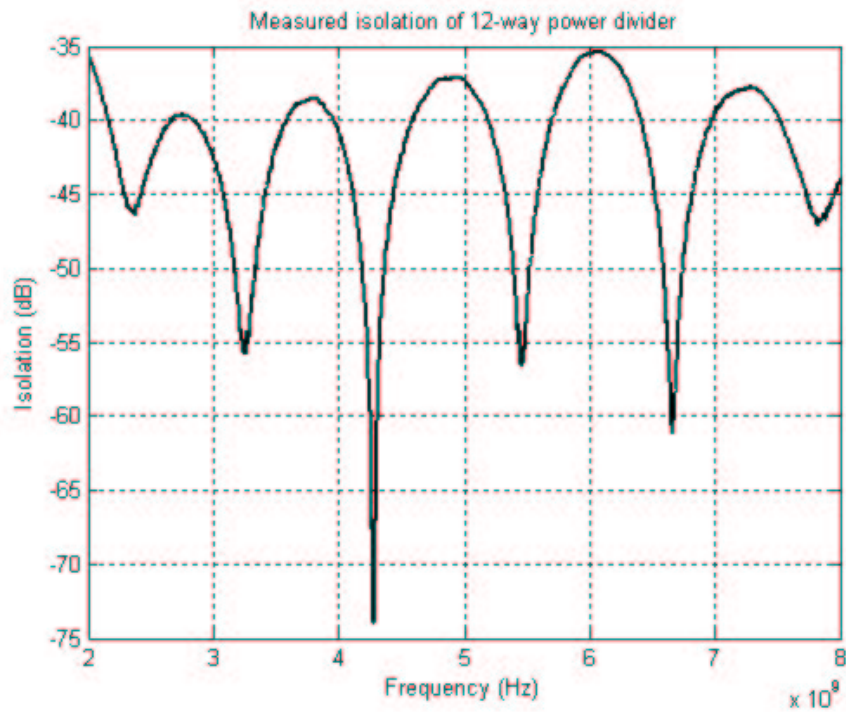
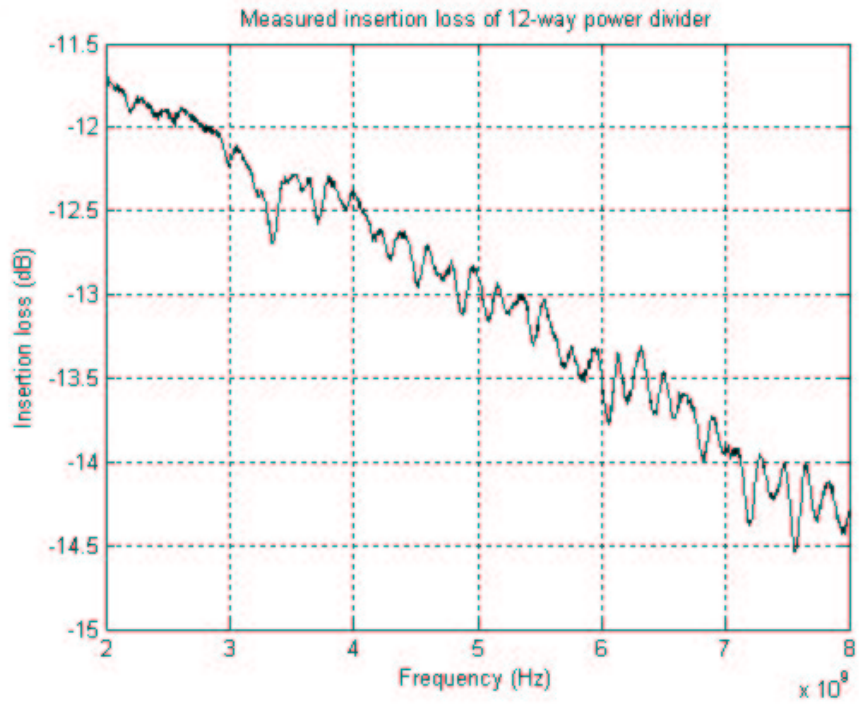


Figure 5-1: Characteristics of 12-way power divider

5.3 Reflection measurements

5.3.1 Test setup

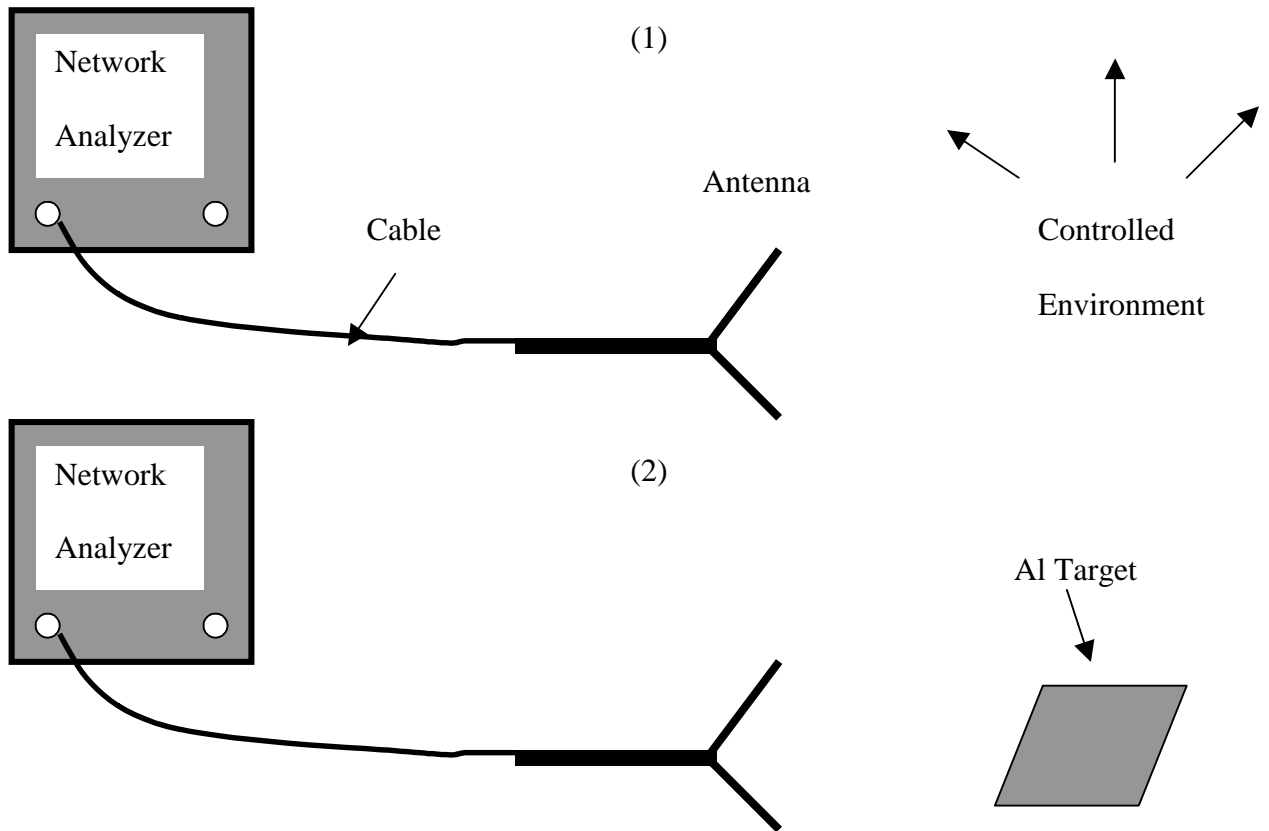


Figure 5-2: S11 measurement setup

The first test that we did was to verify its S-parameters, typically the S11. Figure 5-1 shows the setup for the S11 measurement as well as a reflection test from a metal plate. This gives an idea how well the antenna is matched to the input over the frequency of operation. Ideally, S11 less than -10 dB would be good for an antenna operating over a wide bandwidth. However, this value depends on the kind of application for which the antenna is being designed.

The Network Analyzer (NA) was calibrated to the input of the antenna (or end of the cable) over the 2-8 GHz frequency range. The following sections describe the reflection measurements that were taken with the single element as well as the twelve-element Vivaldi antenna.

Referring to the figure, in the first setup the antenna under test (AUT) was placed outside the building in an environment with minimal clutter. The S11 measurement was then taken. In the second measurement, the antenna was pointed at a flat aluminum plate that was located at various distances from the antenna and the S11 measurements were taken at these points. The reflections from the target at each of these points were then plotted in the time domain to observe the specular target response of the antenna.

5.3.1 Single element Vivaldi antenna

The single element Vivaldi antenna was first connected the Port 1 of the NA and pointed straight ahead, with no major reflector around other than the ground below. The NA was calibrated to sample 201 points over the 2 to 8 GHz frequency range. This corresponds to a maximum unambiguous range of just over 5 meters. In other words, the range to a single target within this distance could be determined without any ambiguity. The S11 measurement vs. frequency was then plotted and compared with the result obtained from the simulation in HFSS as shown in Figure 5-3. It is obvious that the simulation and the measured values match well. Any difference in the two plots could be due to mismatch between the cable and the antenna input as this was not accounted for in the simulation. . The time domain plot (Figure 5-4) of the S11 reveals a lot more interesting facts about the antenna than the frequency plot. The antenna is unmatched to the input port in throughout the bandwidth and hence most of the input power is reflected back from the

antenna itself with very little reaching the outside world. This is clearly evident in the plot near zero range, where the reflections from the antenna are seen as high peaks in the reflection profile. The other values seen across the entire range are reflections coming out of surrounding objects and the ground below.

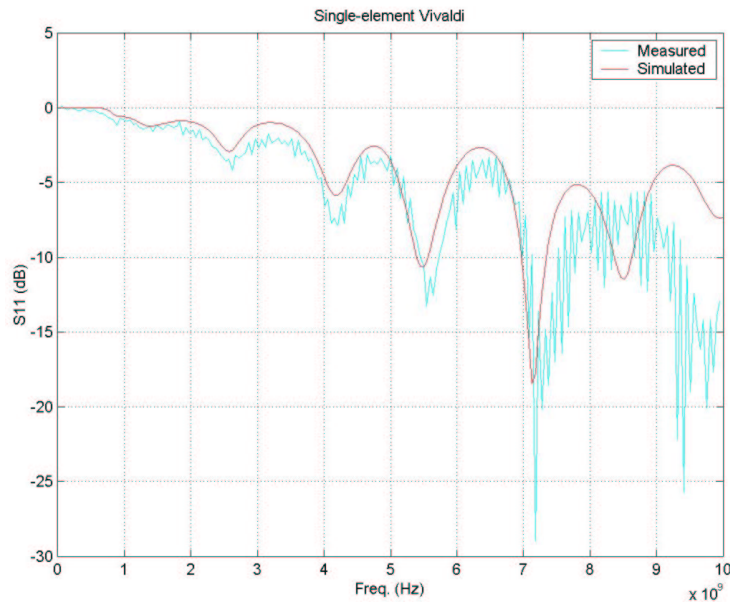


Figure 5-3: S11 comparison

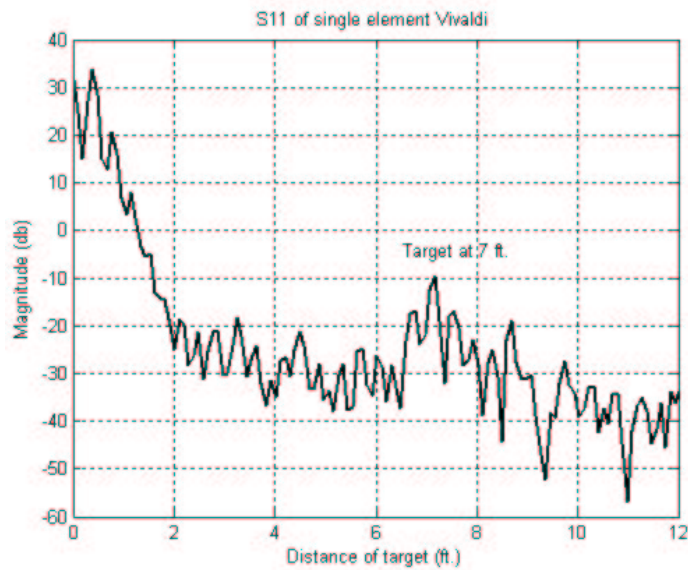


Figure 5-4: Reflection from target at 7ft from antenna

NA Parameter	Setting
Sweep	2-8 GHz
Power output	-10 dBm
Sample points	201
Unambiguous. range	19 ft.

Table 5-1: Network Analyzer settings

Setup 2 was then arranged in the lab to look at the reflections from an aluminum plate on the NA. An input power of -10 dBm is fed into the antenna from the NA. The target was placed at 7 ft. from the outside edge of the antenna and the S11 was measured with the NA. The measured values are then converted to time domain as shown in the Figure 5-4.

Referring to the figure, it can be seen that the reflection from the target is way down in magnitude and almost embedded in the noise floor. Even though the reflection peak from the target aluminum plate is discernible, it is about 44 dB below the peak return. This is mainly because; the gain of the antenna is very low, as predicted by the simulation. The radar equation (given below) could be used to verify this measurement. The received power P_{rec} from a target could be determined as:

$$P_{rec} = \frac{P_{in} * \lambda^2 * G^2 * |\Gamma|^2}{(4\pi)^2 * (2R)^2}$$

where,

$$P_{in} = P_{NA} (1 - |\Gamma|^2)$$

P_{NA} : Network Analyzer output power

Γ : Maximum reflection coefficient

P_{in} : Power input to power divider

G : Gain of the antenna at wavelength λ

P_{rec} = Received power from target

R = Distance between radar and target

P_{NA} (dBm)	λ (m)	$ \Gamma ^2$	P_{ref} (dBm)	G	R (ft)	P_{rec} (dBm)	$P_{ref} - P_{rec}$ (dB) (theoretical)	$P_{ref} - P_{rec}$ (dB) (measured)
-10	0.15	0.76	-11.2	2.5	7	-59	-47.8	-44

Table 5-2: Single element antenna - reflection measurement

From the above table, it is seen that the reflection measurement from the target located at about 7 ft. from the antenna matched its theoretical value with an error of just over 3 dB. This error could be attributed to the inaccurate measurement of the distance between the antenna and the target. Also, the gain of 2.5 was obtained from the HFSS simulation, which could be erroneous. To improve the SNR, the antenna has to have more gain and this was one of the reasons for building an array of Vivaldi elements.

The reflection characteristics of the antenna were thus studied and compared with that of the simulation. The measurements validated the claim made by the simulation that the gain of the single element is quite low.

5.3.2 Twelve-element Vivaldi array

The Vivaldi array was first tested for its reflection characteristics in the lab with the NA. The test setup used with this array is shown. This is just an extension of the single element setup. Since all the 12 elements need to be fed with the input signal, the test port of the NA has to be hooked up to the 12-way power divider. Each output of the power divider is then connected to each of the antenna element in the array. It is important to ensure that the cables connecting to the array elements are of the same length and

characteristics. This assures that there is minimal difference in the amplitude and phase of the input signal fed to each of the antenna elements.

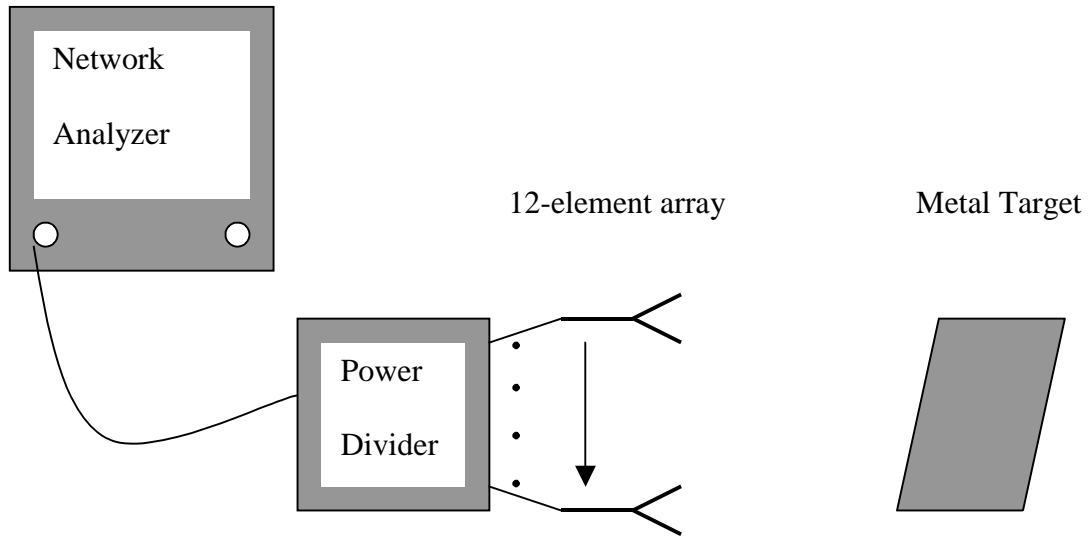


Figure 5-5: Test setup for array antenna

Using a similar setup to the single element antenna test case we measured the reflection from the aluminum plate placed at different distances (3ft., 5ft. and 7ft.)

Figure 5-6: Array reflection measurements

The time-domain plots of the S11 for all three distances are shown in Figure 5-6.

There are several features that are apparent in the figure above:

- The initial feature with the twin peaks is from the input and the output of the power divider respectively.
- The next two features, which have the highest reflections, are reflections from the antenna itself – the first one at the antenna input while the other one from the output of the antenna. The picture of the 12-element array (including the power divider) is shown again here for quick reference.

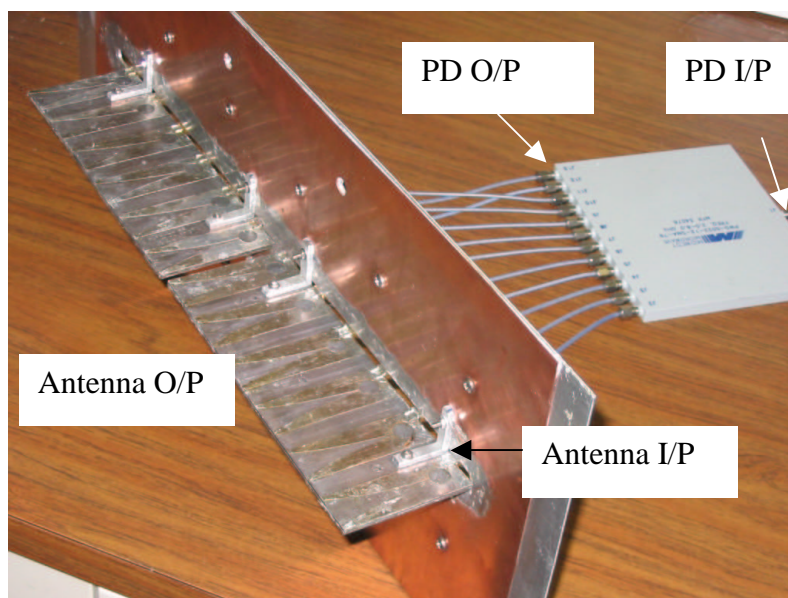


Figure 5-7: Vivaldi array setup

- The subsequent peaks are those of the surrounding objects with the larger ones from the target aluminum reflector placed at different distances. In particular, the ‘green’ peak corresponds to the reflection from the target at about 3 feet away

from the antenna, the 'blue' peak is from the target at 5 feet and the 'red' is from the target located approximately 7 feet from the antenna.

- The following are the differences (in dB) between each of the peak reflections as seen from the NA and depicted in the figure.
 - § Input of the antenna and target at 3 feet: 16.9 dB
 - § Target at 3 feet and at 5 feet: 4.6 dB
 - § Target at 5 feet and 7 feet: 3.4 dB

The reflection profile of the 12-element Vivaldi array antenna measured in the lab contains clutter reflections in addition to the reflection from the mismatch at the antenna input. To determine the S11 of the antenna we will need to filter out the reflection due to clutter. The time-domain plot helps us to identify the regions that we need to remove. A 'Butterworth' bandpass filter of order 5 was used to isolate the antenna reflection. The resultant time signal corresponds to the reflection from the antenna feed and when transformed into the frequency domain, would provide us with the S-parameter (S11) plot for the antenna with respect to frequency as shown in Figure 5-8.

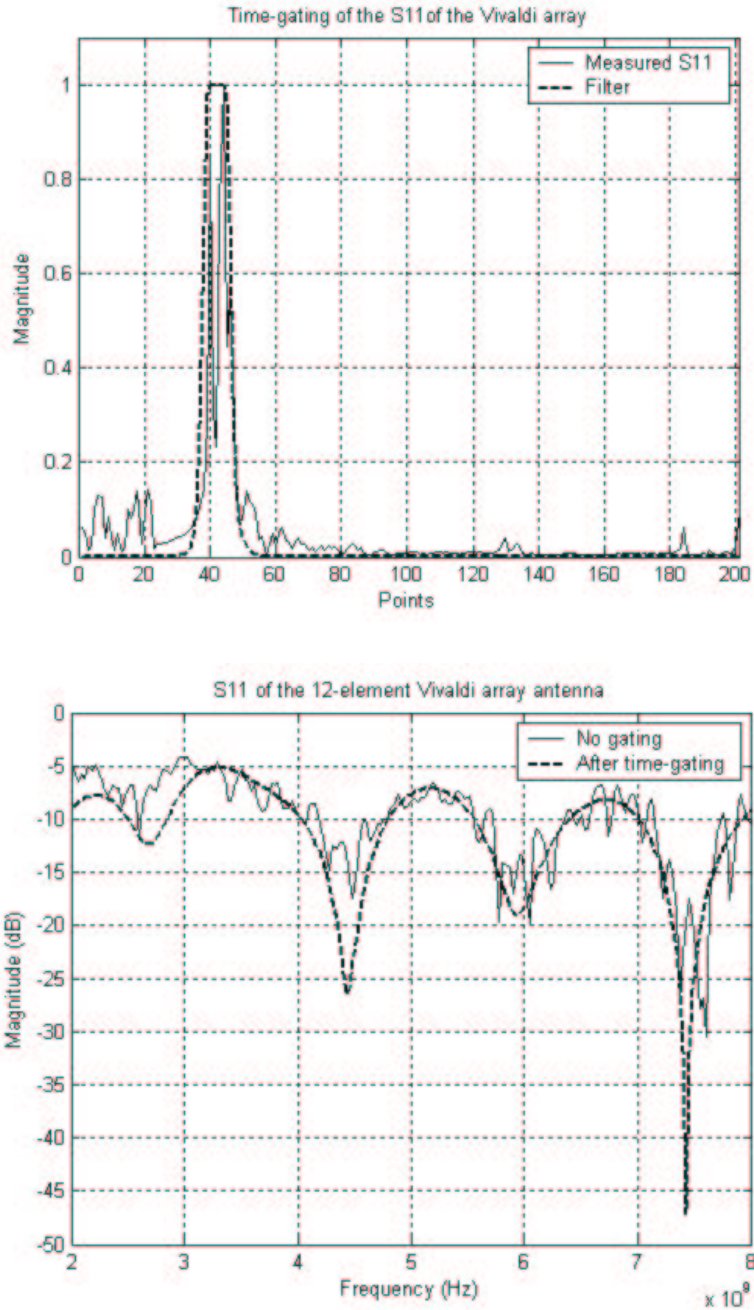


Figure 5-8: Time-gating of reflected signal

Removing the unwanted reflections from the objects in the lab gives us a cleaner frequency-domain plot of the S11 profile. This is essentially the reflection coefficient of the antenna by itself with no outside disturbances. The maximum reflection coefficient

for the antenna is no greater than -5 dB over the entire bandwidth which means that, in the worst case, 68.4% of the input power is actually being transmitted by the antenna.

The next task in hand is to verify if these measurements conform to theory. To do this the calculation of the received power based on the radar range equation was carried out once again.

Going by the worst-case scenario, the maximum reflection coefficient is considered for these calculations. This was observed to occur at a frequency of 2.99 GHz with a magnitude-squared value of 0.405. A simulation was then done in Ansoft HFSS using LBC and the peak gain was found out. It has already been stated that this procedure is really a very crude method of simulating the array. However, this was done purely to aid us in putting down a value for the gain in the radar equation. The exact value for the gain is irrelevant at this stage anyway as we are interested only in the relative magnitude of reflection and not the absolute values. Subsequently, the following parameters are determined from the above relations and settings:

$$P_{in} = P_{NA}(1 - |\Gamma|^2)$$

$$P_{NA} = -10 \text{ dBm or } 10^{-4} \text{ Watts}$$

$$|\Gamma|^2 = 0.405$$

$$P_{in} = 0.595 \times 10^{-4} \text{ Watts}$$

$$G = 27 \text{ at } f = 2.99 \text{ GHz (from HFSS simulation)}$$

$$P_{rec} = \text{received power from reflector}$$

$$R = 3 \text{ ft., } 5 \text{ ft. and } 7 \text{ ft.}$$

The power ratio in each of the cases was then obtained as:

$$10 * \log\left(\frac{P_{antenna}}{P_{3ft}}\right) = 16.93 \text{ dB}; \quad 10 * \log\left(\frac{P_{3ft}}{P_{5ft}}\right) = 4.43 \text{ dB}; \quad 10 * \log\left(\frac{P_{5ft}}{P_{7ft}}\right) = 2.92 \text{ dB}$$

Comparing these values (Table 5-2) to those obtained from the measurement reveals that there is a good agreement between the measured and theoretical predictions.

	Theoretical power ratio	Measured power ratio
Antenna/target at 3 ft	16.93 dB	16.9 dB
Target at 3 ft/target at 5ft	4.43 dB	4.6 dB
Target at 5 ft/target at 7 ft	2.92 dB	3.4 dB

Table 5-3: Power ratio comparison

This concludes the reflection measurements taken with the twelve-element linear Vivaldi array. Based on these measurements, it is clear that the antenna is conforming to the simulated and theoretical expectations.

5.4 Pattern measurements

The knowledge of the exact beam directivity/gain pattern of the antenna will help us in determining the antenna performance in a cluttered environment. The antenna pattern helps us to gauge the amount of clutter that is going to be intercepted and their relative power levels.

5.4.1 Introduction

“An antenna pattern is a graphical representation of the field magnitude at a fixed distance from an antenna as a function of direction”^[30]. Antenna pattern measurements typically consist of the ‘Antenna Under Test’ (AUT) and a standard antenna with a known S11, radiation and polarization characteristics. As a result of reciprocity of transmit and receive patterns of antennas, measurements of gain and radiation patterns can be made with the test antenna used either as a transmitting or a receiving antenna.

But usually, for practical reasons, the AUT is used as a receiving antenna with the transmitting antenna located at a specified location. The source antenna thus provides a constant illumination of the test antenna whose output varies with its angular position. Thus the rule to have in mind is that it is the pattern of the rotated antenna that is being measured. Figure 5-6 illustrates the point just discussed.

A complete representation of the radiation characteristics of the antenna would require measurement at all possible angles. The antenna patterns could be displayed in many possible ways. However, usually only the azimuth and the elevation cuts are performed which provides a good visualization of the actual 3-D pattern of the antenna.



Figure 5-9: Radiation pattern measurement setup

As mentioned earlier, ideally, antenna measurements should be made in free-space conditions. A facility to measure the antenna radiation characteristics is called an antenna range. One of the most important aspects any antenna range is that the source antenna should illuminate a plane wave over the surface of the test antenna. This means that the magnitude and the phase of the incident wavefront must be uniform over the surface of the test antenna. Any deviations from this setup would result in errors in the gain and

pattern measurement. The source should also have sufficient beamwidth so that it is able to illuminate the whole of the test antenna with very little reaching the surroundings and at the same time, not being so narrow that it induces an amplitude taper across the test antenna^[30]. By positioning both the source as well as the test antennas well beyond their respective far-field distances, the spherical wavefront, having traversed so far away from its source, could be assumed as a plane wavefront.

Another major aspect in any antenna range setup is the proximity to potential clutter. This could be a major factor influencing the antenna measurements as a reflection from the ground/objects could interfere with the direct-path signal and cause erroneous nulls/peaks resulting in errors in the measurement. Hence, care should be taken to mount the two antennas as far removed from any obstacles in the vicinity. With the knowledge of the distance between the two antennas, their height above the ground could then be determined such that any multipath signal reaching the test antenna would have no detrimental effect on the received signal.

5.4.2 Setup

The pattern measurements on the Vivaldi array antenna were done at the antenna range facility at KU (KUAR), located on the top of the roof of Nichols Hall. A double-ridged waveguide TEM horn antenna was chosen as the transmit antenna. This antenna was used in the 2003 Antarctica experiment as a part of the Snow Radar. The gain and reflection profile was already known (from datasheets) and hence this was used as the standard antenna.

Before proceeding with the measurements, the far-field distance should be calculated for the test antenna – the 12-element linear Vivaldi array. The minimum range distance

required for the radiating fields to dominate, referred to as the far-field region, is given

by: $r_{ff} = \frac{2D^2}{\lambda}$, where D is the maximum

smallest wavelength of interest. The maximum dimension of the Vivaldi array was found to be 15" (38 cm approx.) and considering the highest frequency of 8 GHz, the far-field distance was found out to be about 7.8 meters.

The KUAR facility was used for the pattern measurements. The facility consists of the following main parts:

- Source and test antenna assemblies on top of the East and the West stairwell towers respectively.
- A Graphic User Interface (GUI) on a PC inside the building that remotely controls the working of the system through connecting cables.

The source and the test antenna mounts in the KUAR facility are separated by a distance of 100 ft (31.4 m), which is greater than the minimum required distance for being in the far-field of the antenna. Hence it could be assumed that the test antenna is illuminated by a plane wavefront. The block diagram of the antenna range setup is shown below.

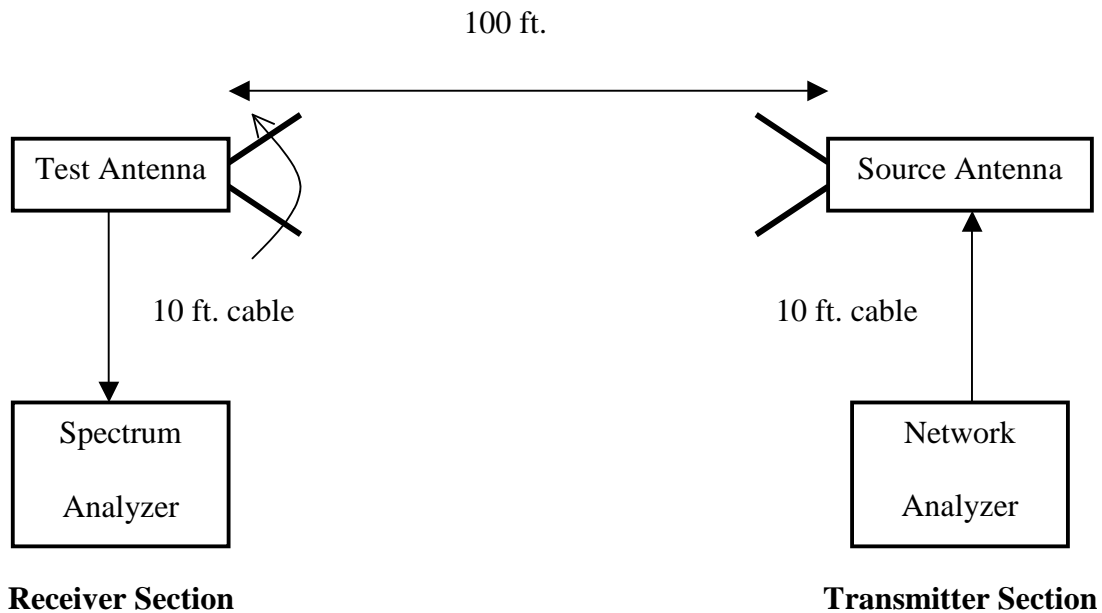


Figure 5-10: Antenna Range setup

The NA - HP 8522D is operated in the continuous-wave (CW) mode at the desired frequency with an output power level of -5 dBm so that it could be used to feed the transmitting antenna. The NA is connected to the transmitting antenna through a 10 feet UTIFLEX cable. At the receiver end, the outputs of the Vivaldi antenna are connected to the power combiner which is connected to a spectrum analyzer (SA) for measuring the power level at the transmit frequencies. The noise floor of the SA is set to a minimum to increase the sensitivity of the spectrum analyzer.

With the above described setup, the three major antenna measurements, viz., polarization, radiation pattern and the absolute gain, were performed. The constituent features of the antenna range setup are listed below. Detailed data sheets on off-the-shelf components listed below have been attached in the Appendix.

Block	Type	Feature
Transmitter	NA HP8522D	CW mode; -5 dBm output power; 2.5, 5, 7.5 GHz
Source antenna	Double-ridged waveguide horn ETS-Lindgren Model 3115	Standard antenna; 1meter Calibrated data available
Receive antenna(s)	(1) 12-element linear Vivaldi array; (2) Same as source antenna	(1) Test antenna (2) Standard antenna for gain measurement
Power divider	Midwest Microwave 12-way PWD-5522-12-SMA-79	Operated as a combiner; 3 dB insertion loss (max); 15 dB isolation
Cables	Utiflex UFA210A; 10 feet	Insertion loss 0.08 dB/ft at 1 GHz and 0.28dB/ft at 10 GHz

Table 5-4: Antenna range setup features

5.4.3 Polarization

It was found from both the simulation (refer Chapter 4) and measurements that the E-field vector was directed horizontal since the element was oriented horizontally. The E-field vectors in fact run between the opposite metal portions of the slotline of the antenna. Most of the power from the antenna is radiated in this particular polarization. However, there is some signal power that is being transmitted with vertical polarization as well. A cross-polarization experiment with a vertically polarized Vivaldi array and a horizontally polarized TEM horn revealed that the signal power was approximately 10-15 dB less than the co-polarized value.

5.4.4 Gain measurement

Most gain measurements are made using an antenna of known gain, called a standard-gain antenna. This technique is generally referred to as the gain comparison method. Having established a suitable range, the signal level with the test antenna in its optimum location is noted. Then the test antenna is replaced with the standard-gain antenna and is placed with its aperture at the center of the location where the test antenna was located. The difference in the received signal power between the standard and the test antenna is computed and is added to or subtracted from the gain of the standard-gain to obtain the gain of the test antenna.

The double-ridged TEM horns were used as the standard-gain antennas with the test antenna being the Vivaldi array. To begin with, the source and the receiver standard-gain antennas were first aligned so that the test antenna was illuminated by the maximum radiation from the source. To achieve this, the receiver antenna was scanned for about 40 degrees on either side of the center and the position where the received power was the highest was noted. This process was repeated for the test antenna for the three desired frequencies - 2.5, 5 and 7.5 GHz. In each case, the peak received power is measured for a transmitted power of -5 dBm.

The gain of the standard-gain antenna was obtained from the calibrated data available from the manufacturers – ETS Lindgren (See Appendix). It should be noted that the absolute gains (as specified in the datasheet) had been determined from a 1.0 meter calibration with horizontal polarization. The calibration is usually done in near-perfect conditions and the gain values could be assumed to be ideal. By connecting this standard-gain antenna on the receiver side, it is possible to compare the gain that we actually

measure with the current range setup to the ideal gain values listed in the datasheet. This would roughly give us an idea as to the error in the system.

The Friis power equation provides us with a method to determine the power received when the transmitted power, gain of the two antennas, their distance of separation and the frequency of operation is known. In the case when both the antennas are of the same type, a little work of algebra will reveal an equation to determine its gain when all the other parameters in the equation are known.

$$P_r = \frac{P_t * G_r * G_t * \lambda^2}{(4\pi R)^2}$$

and, when $G_r = G_t = G$

$$G = \sqrt{\frac{P_r}{P_t}} * \left(\frac{4\pi R}{\lambda} \right)$$

Since both the antennas were connected to the input/output units by 10 feet long cables, it became necessary to take into consideration the loss inherent in them. The attached datasheet of the UTiFLEX cable suggested a loss 0.08 dB/ft at 1 GHz and 0.28 dB/ft at 10 GHz. A linear interpolation was done to obtain the loss for frequencies between 1 and 10 GHz.

The standard TEM horn antenna was then replaced by the AUT at exactly the same position. A similar set of measurements were taken for the Vivaldi array antenna. The inclusion of the power combiner in this setup comes with the insertion loss associated with it. However, this was not included in the gain calculation mainly because of the fact that the power divider was actually a part of the array and in order to look at the antenna as a one-port device, any loss occurring between the feed port of the power divider and the inputs to the individual antenna elements should be disregarded. The results obtained for both the horn and the Vivaldi are shown below.

Frequency (GHz)	Cable loss (dB/ft)	Horn (dBm)	Numeric gain (datasheet)	Numeric Gain (measured)
2.5	0.11	-57.9	8.45	9.65
5	0.17	-62.2	10.37	13.42
7.5	0.23	-66.1	10.64	14.55

Table 5-5: Horn gain measurements

Frequency (GHz)	Cable loss (dB/ft)	Peak received power (dBm)		Peak gain (simulation)	Peak gain (measurement)
		E-plane	H-plane		
2.5	0.11	-60.2	-58.7	16.5	7.65
5	0.17	-68.3	-63.75	36	7.21
7.5	0.23	-64.0	-64.0	40	33.21

Table 5-6: Vivaldi gain measurements

It is obvious that the peak gain at 5 GHz turned out to be at odds with the result obtained from the simulation. This should most probably be due to errors in measurement, both human and otherwise. Having determined the gain of the antenna at the different frequencies, the next step was to perform the radiation plane cuts for the antenna.

5.4.5 Radiation pattern measurements

The radiation pattern is the most demanding in measurement and difficult to interpret among all the antenna measurements. The radiation pattern of an antenna is a three-

dimensional representation of the magnitude, phase and polarization of the radiation emanating from it. Typically, the radiation in two perpendicular planes is measured to get an idea about the field pattern of the antenna. One measurement is done on the plane of polarization and the other in a plane perpendicular to the plane of polarization. The polarization plane is also referred to as the E-plane as it is parallel to the E-field and the latter is described as the H-plane for similar reasons. When taking pattern measurements over real earth, the terms azimuth and elevation are generally used^[32]. In the case of the horizontally polarized Vivaldi antenna, the E-field becomes parallel to the ground and hence the azimuth plane is also the E-plane and subsequently the elevation is the H-plane. Before venturing into the description of the procedure used in taking the pattern measurements, it would be worthwhile exercise to form a prediction of the results for comparison with the measured results. To be more specific: based on the measurements performed in the previous section, the gain of the 12-element Vivaldi could be calculated. Knowing the gain of the TEM horn at the desired frequency, the loss in the cables and the distance of separation between the two antennas, the received power could be arrived at by making use of the Friis transmission equation. The following exercise is for the sole purpose of making an educated guess as to what the received power might be.

$$P_r = \frac{P_t * G_r * G_t * \lambda^2}{(4\pi R)^2}$$

where,

$$P_t = P_{NA} - \text{Cable loss} = -5 \text{ dBm} - 1.7 \text{ dB} = -6.7 \text{ dBm}$$

$$G_r = 10.37 \text{ (from datasheet)}$$

$$G_t = 7.21 \text{ (from measurement)}$$

$$\lambda = 0.06 \text{ m at } f = 5 \text{ GHz}$$

$$R = 100 \text{ ft. (31.4 m)}$$

$$P_r = -64.32 \text{ dBm}$$

$$\begin{aligned} P_{SA} &= P_r - \text{Cable loss} \\ &= -64.32 \text{ dBm} - 1.7 \text{ dB} \\ &= -66.02 \text{ dBm} \end{aligned}$$

The above calculation predicts a received power of -66.02 dBm at the Spectrum Analyzer (SA) for the given specifications.

The setup used to measure the radiation pattern of the Vivaldi antenna has already been described earlier in this chapter. The horizontally polarized Vivaldi (AUT) was operated as the receiver and mounted on top the West tower while the transmitter was the TEM horn mounted on top of the East tower with the same polarization. The transmit power is set as -5 dBm and a continuous wave at the desired frequency is fed to the transmit antenna by the Network Analyzer (NA). The AUT is then rotated in the azimuth direction in desired angle increments and the power received at each increment is noted down from the Spectrum Analyzer (SA). Measurements were taken with two-degree increments for 50° on either side of the major lobe and in five-degree increments for the rest of the scan. This process is carried out for the three frequencies – 2.5, 5 and 7.5 GHz. This concludes the azimuth scan and subsequently the elevation sweep has to be done.

The KUAR does not have the facility to scan the antenna in the elevation direction. Thus the antenna was removed from the current mounting and it was rotated by 90° around the

axis that is the line connecting the two antennas. The antenna was thus oriented perpendicular to the real earth and effectively vertically polarized. If the orientation of the transmit horn antenna is not changed, then any pattern measurement taken subsequently will be one of cross-polarization. Even though this would have been an interesting experiment on its own, it was not pursued further due to the lack of time. To copy the effect of taking the elevation cut, the transmit antenna should also be rotated so that it is also vertically polarized and subsequently we return to taking co-polarization elevation measurements. The vertically polarized AUT was then rotated in the H-plane to obtain the elevation cut. This process is performed with the same NA settings for the same frequencies individually. A total of 240° was swept in both planes for the signal frequencies of 2.5 GHz and 7.5 GHz while for the 5 GHz signal, the azimuth cut was swept for the entire 360° with again a 240° sweep for the elevation plane cut. This was not only done to save time but also for the reason that we were not really interested in knowing about the pattern in the direction diametrically opposite to the main lobe. At each sweep angle the power was measured with the SA. The SA was setup so that the noise floor was well below the signal power level. The receiver bandwidth was set such that even the lowest amplitude signal was discernible.

The “received power versus angle” data obtained from the measurement was loaded into Matlab for further processing. The radiation plots obtained for each frequency is then normalized to the maximum power measured for that frequency. The following are the plots generated from data taken from the pattern measurements done on the roof.

The azimuth cut taken at the frequency of 2.5 GHz is shown below. The antenna was swept over a 110° angle on either side of the center. It is seen that the first side lobe is

close to 13 dB below the main lobe. A HPBW of 23° was observed from the measurement. The gain of the Vivaldi array antenna at this frequency was 8.84 dB.

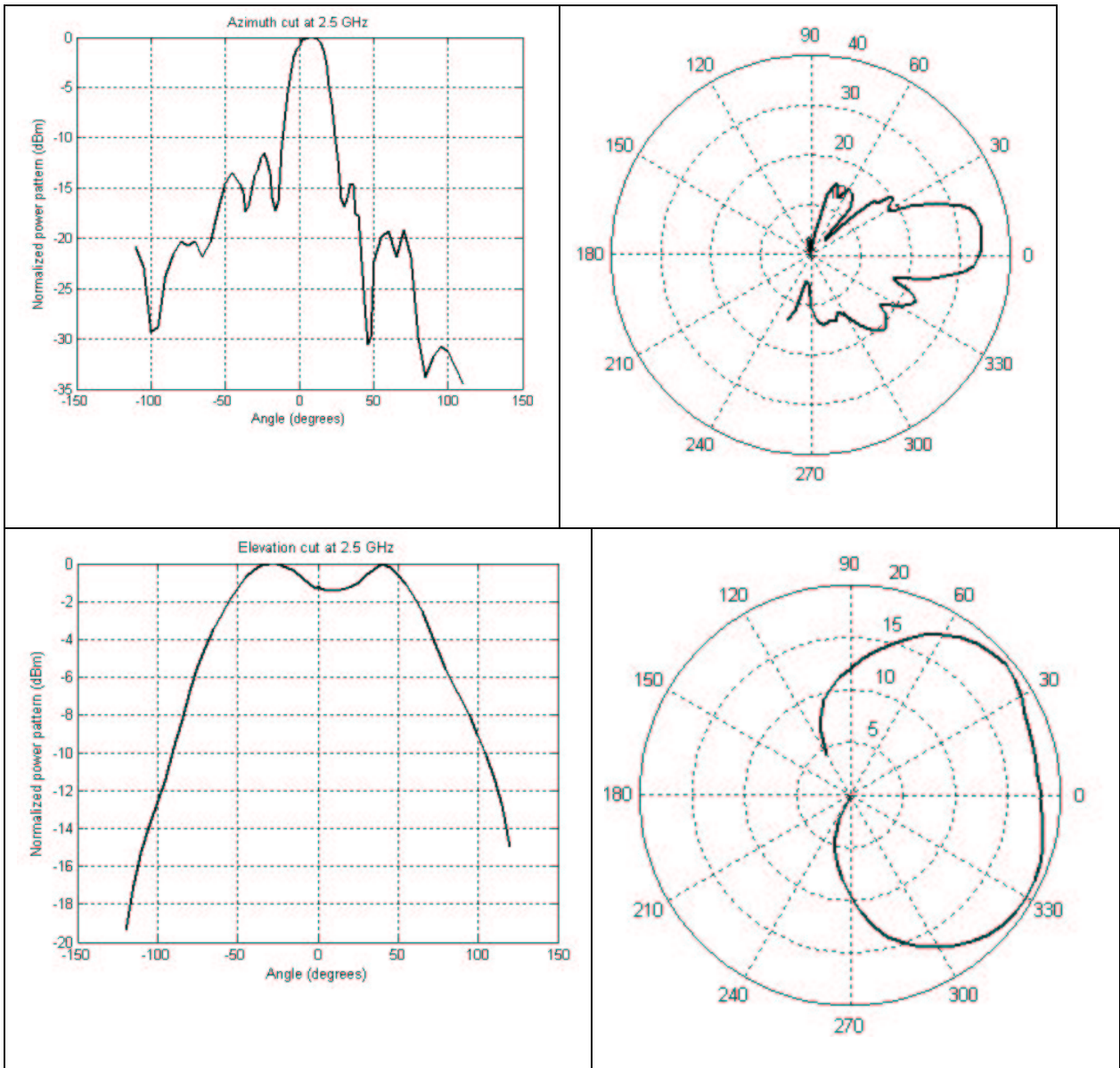
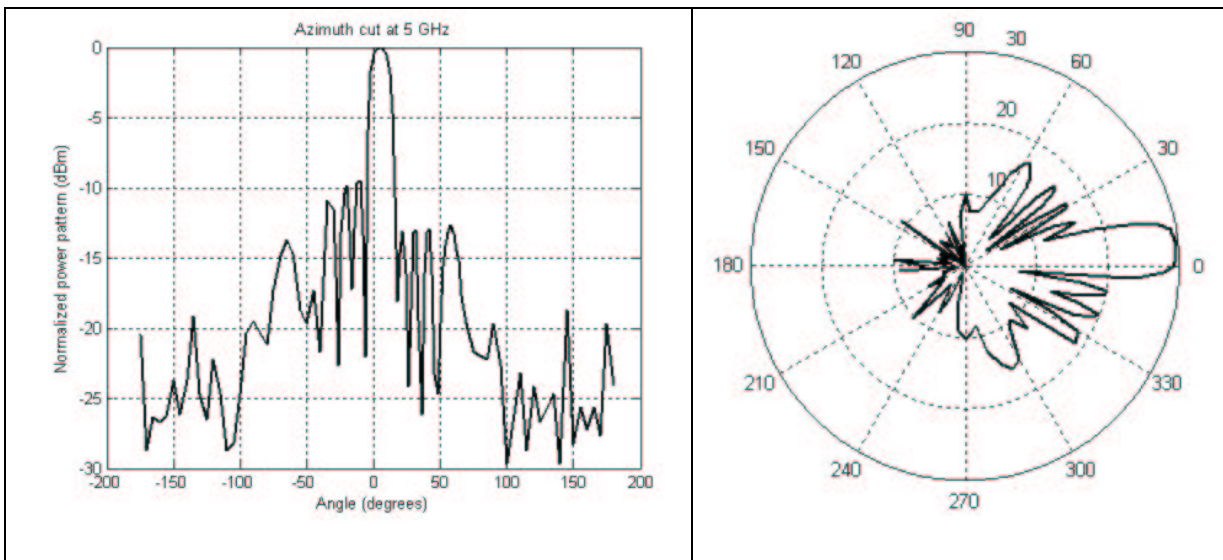


Figure 5-11: Azimuth & Elevation cuts at 2.5 GHz

The elevation cut reveals a broader beam with a HPBW of around 130° with a twin-peak feature suggesting the breaking of the main lobe. In this case, a sweep of 120° on either side of the center position is performed. Also, no side lobes were seen on this sweep.

An azimuth cut at 5 GHz revealed a lot of sidelobes and subsequently the main lobe was fairly narrow. This was generated from a 360° sweep measurement with the Vivaldi array. A HPBW of 14° is obtained from this measurement. The gain realized at this frequency was 8.58 dB. This was below the gain obtained from the simulation by about 7 dB, which is not particularly good. This could probably be due to error in the measurements.

An elevation cut at the same frequency once again gave a wide beamwidth pattern with a HPBW close to 120°. Once again, the twin-peaks are observed on either side of the center position.



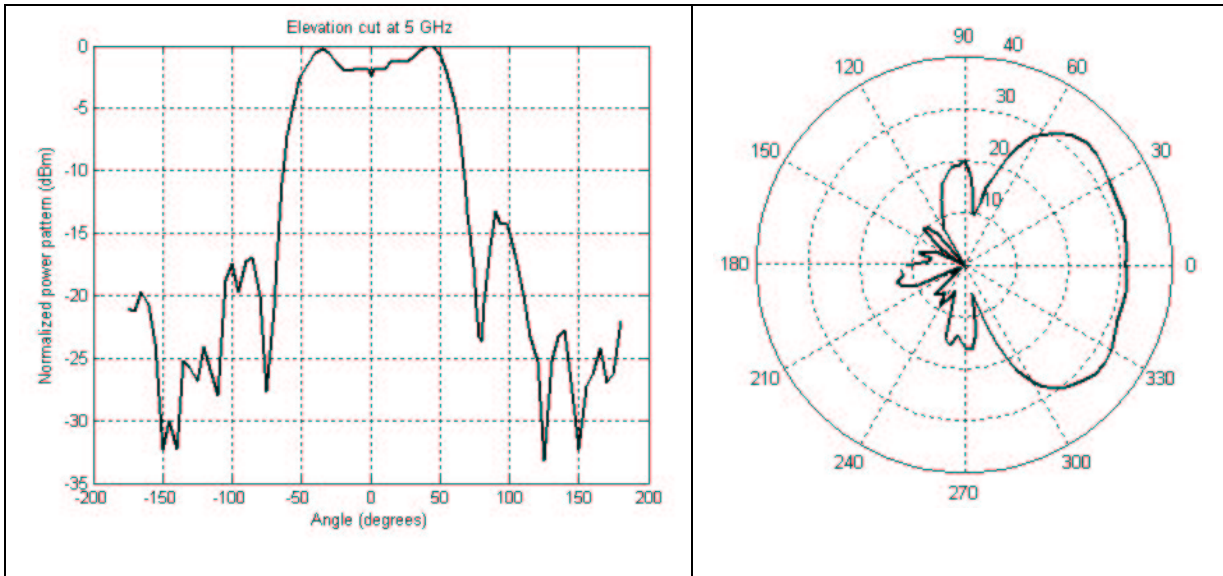


Figure 5-12: Azimuth & Elevation cuts at 5 GHz

The same procedure was repeated for a frequency of 7.5 GHz for both the azimuth and the elevation sweep. The HPBW in the azimuth was still small, with a value of about 12° . The sidelobes increase in number with a corresponding decrease in their magnitude levels. Discrepancies will be explained later in this section. The gain was found out to be 15.21 dB in this case. Finally, the elevation cut for 7.5 GHz is shown below. The HPBW is obtained as 85° . Two sidelobes were observed in the pattern.

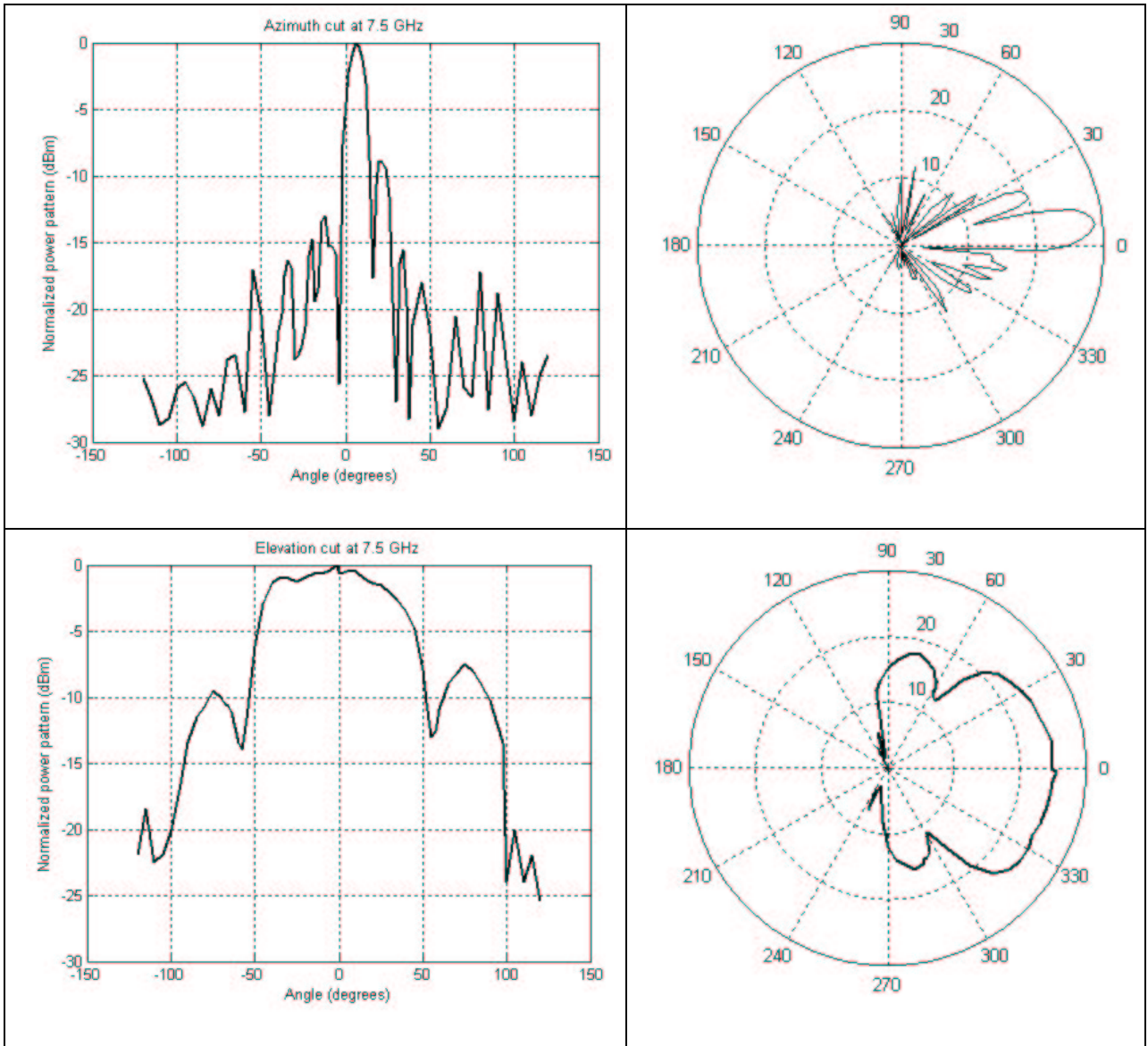


Figure 5-13: Azimuth and elevation cuts at 7.5 GHz

The pattern measurements prove that the beam is really narrow on the azimuth plane or the E-plane while on the perpendicular elevation plane; the beam width is relatively large. This is essentially due to the effect of the configuration of the antenna elements as a linear (1-D) array. The main lobe was effectively centered on the angles 6° to 10°. A 0° center was not obtained due to the inability to align the two antennas exactly on the same

line. This was further affected by extremely windy conditions that resulted in unstable antenna mounts leading to potentially erroneous measurements.

One of the most important causes for errors in the pattern measurements was the presence of the roof floor on one side of the antenna. Moreover, the store room on the roof also caused reflections that got back to the receiver antenna. These concrete structures create multipath signals that could have interfered with the direct path signals in a multitude of ways. This would result in unusually large power at the receiver or on the other hand might also cause severe nulls at points where a particularly high signal power was expected. This could be the reason why the patterns were not symmetrical about the maximum radiation point. Particularly, the sidelobes were not symmetrical with each other. The first sidelobes on either sides of the main beam, in some cases, were not of same magnitude. This means that more power was received on one side of the antenna than the other. Again, the most probable cause would be the effect of multipath signals

5.5 Summary

Antenna measurements form one of the most important aspects of any antenna design. Since the antenna is basically a device radiating in all directions, bench-top measurements become highly error prone. To characterize an antenna, controlled conditions are necessary. Otherwise, the environment would cause potentially severe errors in the measurement. The reflection and the target-return measurements were done in the lab with the NA as the input feed generator and a flat aluminum plate as the target. Time-gating was also accomplished to remove the effect of the surroundings in the S11 measurement. These measurements were done both for the single as well as the array Vivaldi antenna. The pattern measurements were however performed only for the array

antenna. The antenna range on the roof of the building was used for these measurements. A double-ridged TEM horn antenna was used as the immobile standard transmit antenna while the twelve-element Vivaldi array was used as the movable receiving antenna. The movement was controlled remotely from the computer in the lab and the test antenna was rotated in the azimuth direction to obtain the plane cut. The gain and polarization of the antenna were also determined using the same range setup.

The results that were obtained from the different measurements performed with the antenna array are listed below.

Parameter	Value		
S11	<=-7 dB, except for a brief region around 3 GHz		
Polarization	Linear, with E-field lines running between the opposite sides of the slot		
Frequency	2.5 GHz	5 GHz	7.5 GHz
Gain	8.84 dB	8.58 dB	15.8 dB
HPBW E-plane	23°	14°	12°
HPBW H-plane	130°	120°	85°

Table 5-7: Measurement results

Chapter 6 Summary and recommendations

6.1 Summary

The Vivaldi is a member of a class of aperiodic continuously scaled traveling-wave antenna structures. Besides being efficient and lightweight, the more attractive features of this antenna are that it can work over a large frequency bandwidth and produce a symmetrical end-fire beam with appreciable gain and low side lobes. The design of the antenna is very simple and could be completed in the lab with limited resources and labor. This antenna design hence costs less than the horn antenna. Since the antenna worked best in an array, additional beam-forming and adaptive signal processing could be done with this design. These were the basic reasons that led us to investigate the use of the Vivaldi antenna in this particular application.

The antenna was first modeled and simulated using HFSS. Considering frequencies with S11 lesser than -7 dB, the simulation yielded an antenna with a bandwidth of about 10-15%, suggesting that the antenna was primarily unmatched at the port. The model was then fabricated and its S11 was measured in the lab using the Network Analyzer (NA) HP 8722D. It was seen that the simulated and the measured S11 results matched. The simulation revealed a very low antenna gain of 2.48, which subsequently led us to design an array of Vivaldi elements.

The array antenna was modeled in HFSS with a grounded backplane which reflected any signals going in the backward direction. A gain of about 16 dB was obtained for a signal frequency of 7.5 GHz. The array was built and the S11 was measured in the lab. The clutter was gated out and the resulting antenna had close to a 2.5:1 bandwidth, defined for

S11 lesser than -7 dB. This was definitely a marked improvement from the single element case, but of course not good enough. However, “-10 dB bandwidth” definition would reduce the usable bandwidth of the antenna to four chunks of around 1 GHz width each within the desired 2-8 GHz frequency band. This shows that the antenna was not really as wideband as we sought out to be. One of the possible causes for this behavior could be the feed mechanism which was only simulated and not really built and tested. Theoretically, the S11 of the single transition (in the antenna) should have been better than that of the double-transition. However, in practice, exactly the opposite was seen.

Another major issue was that of input impedance matching. Each of the elements had an input impedance of around Z_{in} -point impedance of each of the element in the entire array was not known. A 12-element simulation would have given me an idea about the active impedance. The reflections between the antenna port and the power divider ports should be substantial as to cause a significant amount of loss.

The pattern measurements taken in the roof yielded a peak gain value of around 15 dB (at 7.5 GHz) which was pretty close to the value obtained from simulation. However, the gain at 5 GHz varied by a significantly larger amount (7 dB). This discrepancy might be an error in measurement, because the simulation predicted a steady increase of gain with frequency as is usually the case with most antennas. Also, the pattern cuts were not entirely symmetrical about the main lobe in some of the plane cuts. In fact, in some cases, the main lobe was steeper on one side than the other and in some others; the sidelobes were not symmetrical on both sides. The sidelobes on one side were of larger magnitude than the other, basically due to the fact that more power was received on one of the sides.

This was also probably due to some error in the measurement caused by multipath signals reaching the receiver and interacting with the signal from the direct path. The presence of the roof top and the store room on one side of the antenna range could have resulted in signals being reflected and reaching the receiver out of phase with the direct path signal. Moreover, the experiments were performed in inclement weather and the excessive wind could have changed the orientation of the antennas. Even a slight variation could result in potentially wrong measurements.

The pattern measurements, in general, yielded fairly narrow beamwidths of close to 15° on the E-plane with a wide beamwidth of around 100° on the perpendicular H-plane, which was basically due to setting up the linear array. Such very low beamwidths would greatly benefit the measurement of snow thickness from a large height above the ground, which was one of the aims of this project. Also, the mutual coupling influences the strength of the radiation of the signals from each of the elements. However, a measure of the coupling effects was made impossible with the inability to simulate the full array.

Thus, the twelve-element Vivaldi array was modeled, designed and tested entirely at the lab. The gain of the array seemed to be on the lines of that of the double-ridged waveguide horn that was used as the standard source antenna. Hence, it could readily replace the horn in the current setup of the Snow Radar. A better performance could be attained with a more detailed study of the working of the Vivaldi element and a thorough simulation of the array configuration. This project, I hope, would serve as the first step in using the Vivaldi antenna for effective snow thickness measurement.

6.2 Recommendations

As discussed in the previous section, a lot of improvements / modifications could be done to the design so that better S11 and pattern characteristics could be obtained.

- The feed mechanism should be analyzed more thoroughly. Particularly, by fabricating and testing the transition, it could be found out as to why the single transition behaves worse than the double transition.
- A more powerful computer with a large enough RAM should be used to run the twelve-element simulation. This would enable us to determine the effect of mutual coupling on the driving-point impedance of the array elements. Subsequently, a matching network could be designed so that the ports of the power divider could be matched to the driving-point impedance of each of the element. These two modifications would go a long way in improving the S11 of the antenna and the realized gain of the antenna would also increase correspondingly.
- The pattern measurement process could have been simplified if the automated system was used, rather than manually noting down the readings from the rooftop. However, this required enough amplifiers to boost the signal levels to compensate for the exorbitant loss in the cables. Also, the reflections from the roof floor and the walls could have been time-gated so that their effects do not mask the original signal.
- The process of bonding the two antenna boards together to make the triplate structure involved some real tough procedures that could not be followed strictly in the lab. Having the boards made outside is an option, though costly.

- The measured insertion loss of the power divider matched that of the specifications at the lower side of the frequency range. However, at the higher end of the bandwidth, the insertion loss was worse by 3 dB. A better power divider would have improved the gain of the Vivaldi array significantly

Chapter 7 References

[1] Vinnikov, K. Y., A. Robock, R. J. Stouffer, J. E. Walsh, C. L. Parkinson, D. J. Cavalieri, J. F. B. Mitchell, D. Garrett, and V. F. Zakharov, "Global Warming and Northern Hemisphere Sea Ice Extent," *Science*, vol. 286, 1999, pp. 1934-1937.

[2]

http://earthobservatory.nasa.gov/Newsroom/MediaResources/aqua_sci_writers_guide.pdf

[3] Markus, T. and D. Cavalieri, "Snow Depth Distribution over Sea Ice in the Southern Ocean from Satellite Passive Microwave Data. Antarctic Sea Ice: Physical Processes, Interactions, and Variability," *Antarctic Research Series*, Washington, DC, 74:19-39, 1998.

[4] Wong: "Development of a Prototype of a 2-8 GHz FMCW Radar for Snow Thickness Measurement on Sea Ice," *M.S Thesis*, University of Kansas, 2003.

[5] Gibson, P.J., "The Vivaldi aerial," *Proc. 9th European Microwave Conference*, 1979, pp. 103-105.

[6] <http://www.ansoft.com>

[7] H.Y. Wang et al, "Rigorous analysis of Tapered Slot Antennas on dielectric substrates," *10th International Conference on Antennas and Propagation*, 1997.

[8] R. Janaswamy and D.H. Schaubert, "Analysis of a Tapered Slot Antenna," *IEEE Transactions on Antennas and Propagation*, Vol. AP-35, No. 9, September 1987, pp. 1058-1065.

[9] Yngvesson et al, "The tapered slot antenna – A new integrated element for millimeter-wave applications," *IEEE Transactions on Microwave Theory and Techniques*, Vol. 37, No. 2, February 1989, pp. 365-374.

- [10] Oraizi and Jam, "Optimum design of TSA profile," *IEEE Trans. on Antennas and Propagation*, Vol. 51, No. 8, August 2003, pp. 1987-1995.
- [11] H. Jasik, *Antenna Engineering Handbook*, McGraw-Hill, 1961.
- [12] R.Q. Lee and R.N. Simons, "*Advances in Microstrip and Printed Antennas*," John Wiley and Sons, 1997.
- [13] R.Q. Lee and R.N. Simons, "Effect of Curvature on Tapered Slot Antennas," *Antennas and Propagation Society International Symposium*, 1996, AP-S. Digest , Vol.1, pp. 188 –191.
- [14] J.P. Weem et al, "Vivaldi antenna arrays for SKA," *Antennas and Propagation Society International Symposium*, Vol.1, July 2000, pp. 174-177.
- [15] K.C. Gupta, R. Garg and I.J. Bahl, "Microstrip Lines and Slotlines," *Artech House*, Dedham, MA, 1979.
- [16] Knorr, J.B., "Slotline transitions," *IEEE Trans.*, Vol. MTT-22, 1974, pp. 548-554.
- [17] Weedon et al, "A step-frequency radar imaging system for microwave nondestructive evaluation," *Progress in electromagnetic research*, 2000, pp. 121-146.
- [18] Schuppert, "Microstrip/slotline transitions: Modeling and experimental investigations," *IEEE Trans.*, Vol. MTT-36, 1988, pp. 1272-1282.
- [19] A. H. Atwater, "The Design of the Radial Line Stub: A Useful Microstrip Circuit Element," *Microwave Journal*, Vol. 28, 1985, pp.149-156.
- [20] Sloan et al, "A broadband microstrip-to-slotline transition," *Microwave and optical technology letters*, Vol. 18, No. 5, August 1998, pp. 339-342.
- [21] Gazit, "Improved design of a Vivaldi antenna," *IEEE Proc. H*, 1988, pp 89-92.

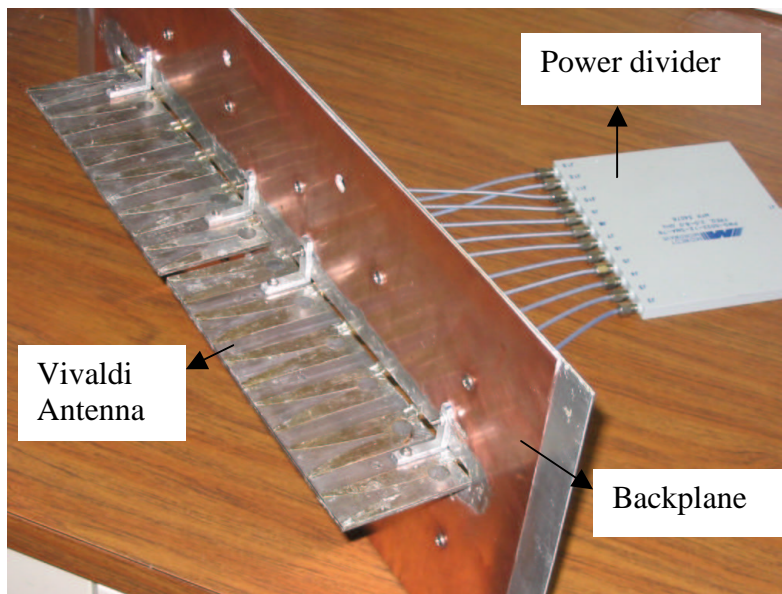
- [22] Noronha et al, "Designing antennas for UWB systems," *Microwaves & RF Journal*, June 2003, pp. 53-61.
- [23] Langley et al, "Novel ultrawide-bandwidth Vivaldi antenna with low cross-polarization," *Electronic Letters*, Vol. 29, No. 23, 1993, pp. 2004-2005.
- [24] The 2000 CAD Benchmark, *Microwave Engineering Europe*, <http://img.cmpnet.com/edtn/europe/mwee/pdf/CAD.pdf>
- [25] Schaubert & Shin, "A parameter study of stripline-fed Vivaldi notch-antenna arrays," *IEEE Trans. on Antennas and Propagation*, Vol. 47, No. 5, May 1999, pp. 879-886.
- [26] Advanced circuit materials - Technical Tips, Rogers Corporation website, <http://www.rogerscorporation.com/mwu/techindx.htm>
- [27] Bhartia et al, "Microstrip Antenna Design Handbook,"
- [28] Wadell, "Transmission Line Design Handbook," *Artech House*, 1991.
- [29] Taflove and Thiele, "FD-TD analysis of Vivaldi flared-horn antennas and arrays," *IEEE Trans. on Antennas and Propagation*, Vol. 42, No. 5, May 1994, pp. 633-641.
- [30] Stutzman and Thiele, "Antenna theory and design," 2nd Edition, *John Wiley & Sons*, 1998.
- [31] Dr. Pannirselvam Kanagaratnam, Research Assistant Professor, Electrical Engineering and Computer Science, The University of Kansas, Lawrence.
- [32] Turin, "The ARRL Antenna Book," 19th Edition, Chapter 28, pp. 46-52

Chapter 8 Appendix

8.1 Datasheets

Part	Datasheet
Rogers Substrate	http://www.rogerscorporation.com/mwu/pdf/5000data.pdf
Power divider	http://ebiz.midwest-microwave.com/cgi-bin/mmb2c/PWD-5522-12-SMA-79.html
UTiFLEX Cables	http://www.micro-coax.com/utiflex/utiflex_lowloss.htm
Double-Ridged Waveguide horn	http://www.ets-lindgren.com/Manuals/3115.pdf

8.2 Pictures



(a)



(b)

Figure 8-1: Vivaldi antenna array in (a) Horizontal, and (b) Vertical polarization

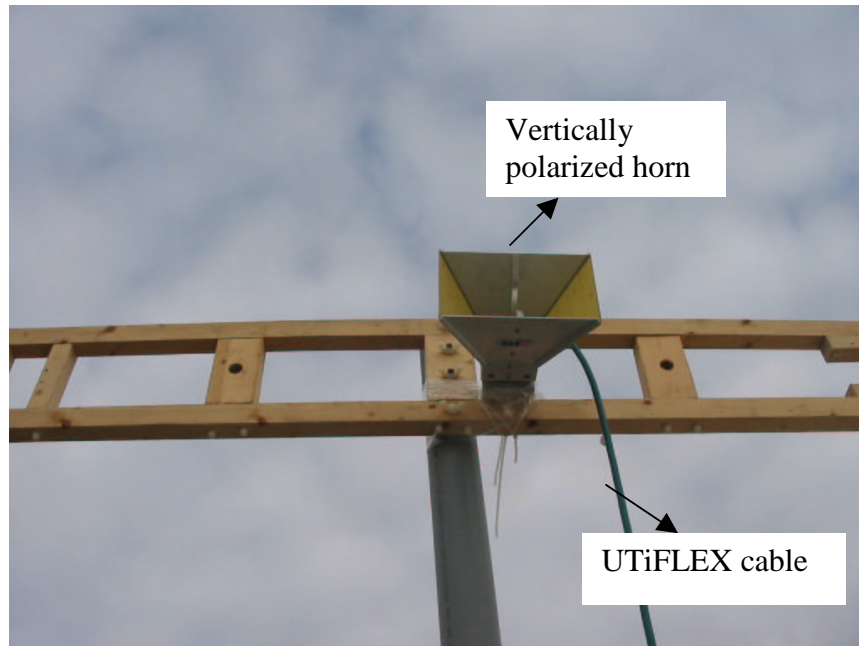


Figure 8-2: Double-ridged waveguide horn - Vertically polarized

